MATERIALE PLASTICE
https://revmaterialeplastice.ro
https://doi.org/10.37358/Mat.Plast.1964

CC BY

Surface roughness optimization of FFF-printed carbon fiber-reinforced nylon using entropy-TOPSIS, PCA–TOPSIS and machine learning techniques

SUBHASH SELVARAJ[1]*, RAJESH P. K.[2]
[1] Department of Mechanical Engineering, EASA College of Engineering and Technology, Coimbatore, India
[2] Department of Automobile Engineering, PSG College of Technology, Coimbatore, India

Abstract: *Surface roughness is one of the major challenges in parts produced by Fused Filament Fabrication (FFF) because of the staircase effect created during layer-by-layer fabrication. This study focuses on minimizing the surface roughness of FFF-printed nylon composites reinforced with 20% carbon fiber using a combination of Taguchi design, Multi-Criteria Decision-Making (MCDM) techniques, and Machine Learning (ML) algorithms. Five process parameters, namely build orientation, layer thickness, infill density, raster angle, and infill pattern, were varied at different levels using a Taguchi L_{18} experimental design. Surface roughness parameters, namely arithmetical mean height of the roughness profile (Ra) and maximum height of the roughness profile (Rz), were measured in two perpendicular directions using a MarSurf VD280 surface profilometer. The experimental results were first analyzed using the Signal-to-Noise (S/N) ratio method. Signal-to-noise analysis identified layer thickness as the most influential factor within the investigated parameter space, while MANOVA indicated a significant multivariate association of layer thickness with the combined surface roughness responses under the fitted main-effects model (Wilks' Lambda, $p = 0.033$). Multi-response optimization was then carried out using a comparative Entropy-TOPSIS and PCA–TOPSIS approaches to identify the optimal process settings for improved surface quality. The resulting multi-response performance index was further used to train and evaluate several regression-based machine learning algorithms with different train-test split ratios (60:40, 70:30, 80:20, and 90:10). Among the algorithms tested, the AdaBoost regression model showed the best predictive performance with a maximum coefficient of determination (R^2) value of 0.99. The analysis revealed that layer thickness was the most influential parameter affecting surface roughness. Surface characterization using Scanning Electron Microscopy (SEM) confirmed the presence of voids and surface irregularities in the printed specimens. The proposed hybrid optimization and prediction framework demonstrates an effective approach for improving the surface quality of carbon fiber reinforced nylon components manufactured through FFF.*

Keywords: *Entropy, principal component analysis, TOPSIS, Adaboost algorithm, signal to noise ratio*

1. Introduction

Additive Manufacturing (AM) technologies, particularly Fused Filament Fabrication (FFF) have gained significant attention across various industrial sectors, including aerospace, biomedical engineering, mold manufacturing, and automotive applications, owing to their capability to fabricate components ranging from simple visual prototypes to complex aerospace drilling fixtures [1,2]. FFF has emerged as one of the most widely adopted AM processes due to its low material, operational, and maintenance costs, as well as its ability to manufacture geometrically complex and multifunctional components [3]. The FFF process fabricates parts layer by layer based on machine instructions generated from a sliced STL model. Despite its advantages, FFF-produced parts often exhibit inferior mechanical properties, poor surface finish, and dimensional inaccuracies when compared with conventionally manufactured

email: subhashraj18@gmail.com

components produced through processes such as injection molding and compression molding [4]. Consequently, numerous studies have focused on optimizing FFF process parameters to improve mechanical properties such as tensile strength [5,6] and flexural strength [7], enhance surface quality [8–10], and reduce dimensional deviations [11–13]. In addition to process optimization, post-processing techniques have also been explored to further improve the mechanical performance, surface characteristics, and dimensional accuracy of FFF-fabricated parts [14–16]. FFF components are generally characterized by multiple performance responses, making process optimization a challenging task. Improving one response may adversely affect another, thereby limiting the broader industrial adoption of the technology for mass production. This challenge highlights the need for multi-response optimization approaches that can simultaneously satisfy multiple quality requirements. Multi-response optimization has been successfully applied in various fields, including machine and material selection [17,18], additive manufacturing process selection [19], solar power plant site selection [20], financial management [21], and machining parameter optimization [22].

Multi-Criteria Decision-Making (MCDM) techniques provide effective tools for solving problems involving multiple and often conflicting objectives. Advances in computational mathematics have further simplified the implementation of MCDM methods for complex engineering applications. Researchers have employed both criteria-weighting and alternative-ranking approaches to identify optimal parameter combinations that satisfy multiple performance requirements. Prabhu et al. [23] integrated TOPSIS and fuzzy expert systems to minimize shrinkage and warpage in FFF components. Their findings revealed that layer thickness had a significant influence on the responses, whereas print speed exhibited relatively low significance. The fuzzy expert model predicted shrinkage allowances with an error of less than 5%. Similarly, Saad et al. [24] investigated the optimization of surface roughness in PLA components fabricated through FFF using Response Surface Methodology (RSM), Particle Swarm Optimization (PSO), and Symbiotic Organism Search (SOS) algorithms. The prediction errors of PSO and SOS were reported to be below 8.8%. Mohanty et al. [25] employed a hybrid Taguchi–MARCOS framework integrated with nature-inspired algorithms to minimize dimensional variations in ABS M30 components. Among the parameters studied, part orientation emerged as the most influential factor affecting dimensional accuracy. Qin et al. [26] adopted a three-way decision-making model for material selection in metal additive manufacturing applications. Vinodh and Shinde [27] compared MOORA and TOPSIS approaches for optimizing FFF parameters with respect to surface finish and build time and observed identical ranking orders from both methods. Their study identified layer thickness and infill pattern as critical factors affecting part quality.

Chinchanikar et al. [28] optimized infill density, layer height, print speed, and extrusion temperature to simultaneously improve tensile, impact, and flexural strengths while reducing surface roughness in PLA components. They utilized hybrid optimization techniques including TOPSIS, NSGA-II, and Desirability Function Analysis coupled with RSM, and Grey Relational Analysis (GRA), achieving prediction errors below 10%. Rajamani et al. [29] improved the surface quality of an FFF-fabricated flapping-wing aeromechanism assembly using a hybrid RSM–TOPSIS approach. Sakthivel Murugan and Vinoth [30] optimized FFF process parameters for an automotive component using GRA, AHP, and TOPSIS methods, reporting significant similarities between the ranking results obtained from different techniques. More recently, Mohammed Raffic et al. [31] integrated MCDM techniques with machine learning algorithms to identify optimal process parameters for maximizing a combined performance index. Their study demonstrated that Decision Tree and AdaBoost algorithms outperformed other machine learning models when evaluated using an 80:20 train-test split ratio. Selvaraj and Rajesh [32] predicted the optimal parameters for minimizing the geometrical deviations in carbon fiber reinforced nylon filaments through Entropy-CoCoSo and PCA-TOPSIS techniques. The experimental dataset has been assessed through classification algorithms and Naïve bayes algorithm outperformed other algorithms with a classification accuracy of 99.4%.

The literature review indicates that MCDM techniques are highly effective for multi-response optimization of FFF process parameters. However, studies focusing on carbon fiber reinforced nylon composites through MCDM based optimization combined with machine learning frameworks for surface roughness minimization remain limited. Therefore, the present study investigates the multi-response optimization of FFF process parameters, namely build orientation, layer thickness, infill density, raster angle, and infill pattern, with the objective of minimizing surface roughness measured in two perpendicular directions. Except for build orientation, which is varied at two levels, all other parameters are considered at three levels. An L_{18} Taguchi orthogonal array comprising eighteen experimental trials is developed using Minitab 17.0 software. Criteria weights are determined using Entropy and Principal Component Analysis (PCA) methods, while alternative ranking is performed using the TOPSIS technique. Furthermore, the resulting multi-response performance index is analyzed using regression-based machine learning algorithms with different train-test split ratios to identify the most suitable predictive model.

2. Materials and methods

The current section sheds light about the filament material and FFF printer utilized in the current study. The technique behind the creation of experimental layout is also detailed in the current section.

2.1. Filament material

For sample preparation, filament of 1.75 mm diameter consisting of nylon 6/66 copolymer as the matrix phase and 20% carbon fiber as the reinforcing material supplied by Esun, China, was considered. The properties of the material make it suitable for the production of industrial parts and gears, which need higher strength and stiffness. Tensile strength of the filament material is 140 MPa and the density is 1.24 g/m^3 [32].

2.2. 3D printer

The Flashforge Creator Pro 3 professional FFF printer (made in China) is used to prepare the sample. It includes a twin extruder for filament extrusion and a total construction volume of 300 × 250 × 200 mm. The machine can print a variety of filament materials, including PLA, ABS, PA, PC, PVA, HIPS, PETG, wood, ASA, and their fiber-reinforced composite filaments, with a maximum extrusion temperature of 300°C. With regard to the filament extruded, the extrusion nozzle's diameter can be changed to 0.4, 0.6, and 0.8 mm [32].

2.3. Experimental design

The experimental design for the present study was developed using Taguchi's orthogonal array methodology with the aid of Minitab 17.0 software. The Taguchi L_{18} orthogonal array was selected because the present study involved one two-level factor (build orientation) and four three-level factors, making L_{18} the most suitable mixed-level orthogonal array while minimizing the number of experimental trials. The objective of this investigation was to identify the principal effects of process parameters rather than develop a complete interaction model. A mixed-level fractional factorial design was adopted by considering five FFF process parameters: build orientation, layer thickness, infill density, raster angle, and infill pattern. Among these factors, build orientation was evaluated at two levels, while the remaining four parameters were investigated at three levels each. Figure 1a–c represents the raster angles 0°, 45° and 90° degrees, respectively. Based on the selected factor-level combinations, a total of eighteen experimental runs were generated using the Taguchi L_{18} orthogonal array. Table 1 presents the selected FFF process parameters along with their corresponding levels, whereas Table 2 illustrates the complete experimental matrix comprising the eighteen trials obtained from the mixed-level fractional factorial design [32].

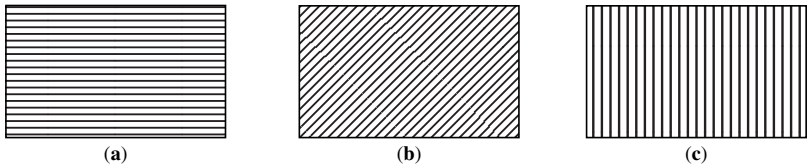


Figure 1. Raster angle at different directions (**a**) 0°, (**b**) 45° and (**c**) 90°

Table 1. FFF input parameters and their levels [32]

S. no.	Input parameter	Symbol	S.I unit	Level 1	Level 2	Level 3
1	Build orientation	A	–	Flat	On edge	–
2	Layer thickness	B	mm	0.1	0.17	0.24
3	Infill density	C	%	50	75	100
4	Raster angle	D	°	0	45	90
5	Infill pattern	E	–	Cubic	Triangles	Grid

Table 2. Taguchi L18 experimental matrix with input factors in uncoded units [32]

Trial no.	A	B (mm)	C (%)	D (°)	E
1	Flat	0.1	50	0	Cubic
2	Flat	0.1	75	45	Triangles
3	Flat	0.1	100	90	Grid
4	Flat	0.17	50	0	Triangles
5	Flat	0.17	75	45	Grid
6	Flat	0.17	100	90	Cubic
7	Flat	0.24	50	45	Cubic
8	Flat	0.24	75	90	Triangles
9	Flat	0.24	100	0	Grid
10	On edge	0.1	50	90	Grid
11	On edge	0.1	75	0	Cubic
12	On edge	0.1	100	45	Triangles
13	On edge	0.17	50	45	Grid
14	On edge	0.17	75	90	Cubic
15	On edge	0.17	100	0	Triangles
16	On edge	0.24	50	90	Triangles
17	On edge	0.24	75	0	Grid
18	On edge	0.24	100	45	Cubic

3. Experimental work

The experimental samples have been prepared through Flashforge Creator 3 Pro FFF printer and its specifications are shown in Table 3. The experimental samples have been prepared from Nylon 6/66 filament reinforced with 20% carbon fiber. The printer has a build volume of 300 × 250 × 200 mm and can produce components with layer heights in the range of 0.05 to 0.40 mm. The filament has been extruded at a temperature of 280°C with a bed temperature of 80°C in order to enhance the initial layer adhesion with the printed bed surface. The filaments have been deposited at a rate of 100 mm/s and the samples are printed in accordance with ASTM D2240 standard with a dimension of 25 × 20 × 6.4 mm. The prepared sample can be adopted for evaluating the dimensional accuracy of a simple geometry printed through FFF process and also the Shore D hardness value.

Table 3. 3D printer specification

S. no.	Specification	FlashForge creator 3 Pro
1	Printing technology	Fused Filament Fabrication (FFF)
2	Extruders	2 independent extruders
3	Build volume	300 × 250 × 200 mm
4	Filament diameter	1.75 mm
5	Standard nozzle diameter	0.4 mm
6	Layer-height capability	0.05–0.40 mm
7	Printing speed	10–150 mm/s
8	Printing accuracy	±0.2 mm
9	XY positioning accuracy	0.011 mm
10	Z positioning accuracy	0.0025 mm

The filament was visually inspected for contamination and dimensional irregularities before printing. Since the nylon-based materials are moisture sensitive, filament was stored under controlled conditions and dried prior to printing where applicable to reduce the effect of absorbed moisture on the stability of extrusion and surface quality. The filament was then loaded into the designated extruder and the extrusion path was checked to ensure continuous and uniform material deposition. The specimens were designed as rectangular specimens suitable for surface roughness characterization. The three-dimensional specimen model was converted into an STL file and subsequently imported into the slicing software. The slicing operation was performed by defining the required build orientation, layer thickness, infill density, raster angle, and infill pattern according to the Taguchi L_{18} experimental design. Thus, each experimental trial corresponded to one unique combination of the five selected FFF process parameters. For each trial, the corresponding parameter combination was entered into the slicing software and the sliced model was converted into the machine-readable toolpath required by the FFF printer. The specimen was positioned on the build platform according to the prescribed build orientation. The printer was then allowed to complete the deposition of the specimen layer by layer. Except for the five parameters intentionally varied in the experimental design, all other printing conditions were maintained constant throughout the experimental programme in order to minimize uncontrolled process variation. After completion of printing, the specimens were allowed to cool to room temperature before being removed from the build platform. No machining or surface-finishing operation was performed on the surfaces intended for roughness evaluation, since such operations could alter the actual surface characteristics produced by the FFF process. Each specimen was identified according to its corresponding Taguchi trial number to prevent interchange of samples during subsequent measurements.

The surface roughness of the fabricated rectangular specimens was measured using a MarSurf VD280 surface measurement system at two different locations on each sample. The instrument is capable of measuring both surface roughness and contour profiles over a measuring length of up to 280 mm, with measurement speeds ranging from 0.02 mm/s to 10 mm/s. Figure 2 illustrates the 3D-printed specimens used for surface roughness evaluation, while Figure 3 depicts the two measurement directions considered in the study.

Surface roughness measurements were performed using a Mahr MarSurf VD280 surface measurement system equipped with a CPG T 12-210-25/12° diamond stylus probe. The stylus had a nominal tip radius of 25 μm and an included tip angle of 12°. The probe arm had a nominal length of 210 mm and was operated in the downward tracing direction. A tracing speed of 0.50 mm/s was employed. The roughness profile was evaluated using a Gaussian filter with a cut-off length (λc) of 0.8 mm and an evaluation length of 11.51 mm. The total tracing length recorded by the instrument was **16.57 mm**, while the reported evaluation length was **11.51 mm**. The measurement data were processed using the

MarTalk/MarWin software environment. The roughness parameters **Ra** and **Rz** were extracted from the evaluated profile. Measurements were conducted along two mutually perpendicular directions on each specimen, and the corresponding values were averaged for subsequent analysis.

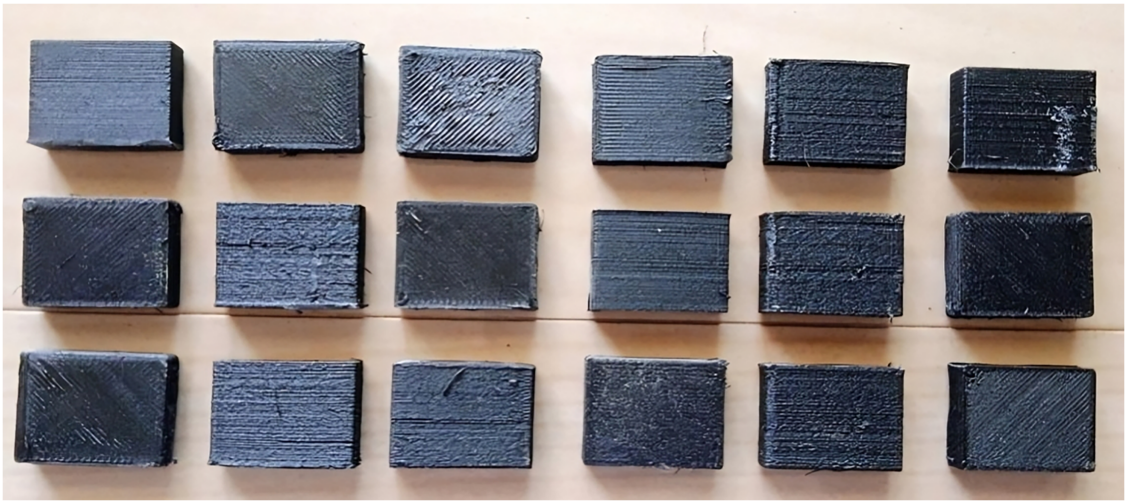


Figure 2. Samples for measuring surface roughness

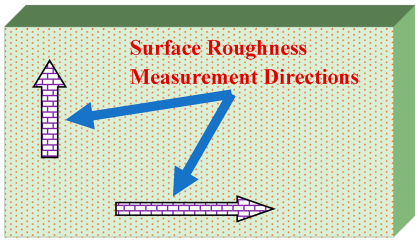


Figure 3. Surface roughness measurements at different directions in sample

Surface roughness parameters, namely arithmetical mean height of the roughness profile (Ra) and maximum height of the roughness profile (Rz), are widely employed to assess the surface quality of manufactured components [33]. To evaluate the influence of FFF process parameters on surface characteristics, Ra and Rz values were measured in both the horizontal and vertical directions of each specimen. As no replicate specimen has been prepared in the study, for each specimen, Ra and Rz were measured at three randomly selected points along each of two mutually perpendicular directions (horizontal and vertical). The three measurements obtained in each direction were averaged separately to obtain the representative directional value. The final Ra and Rz values for each experimental condition were then calculated by averaging the representative values obtained from the two directions. Thus, each reported experimental value was based on six individual measurements per specimen, comprising three measurements in each of the two measurement directions. These repeated measurements represent measurement-level repetitions within the same specimen and were not treated as independent experimental specimen replications. The absence of independent specimen replication limits the ability to estimate pure experimental error separately from other sources of residual variation, and the statistical results are therefore interpreted primarily within the investigated experimental design space.

The average values obtained from the two measurement directions were used for subsequent analysis and also in optimization. Figure 4 presents the MarSurf VD280 system utilized for surface roughness

measurement in the present study and Table 4 represents the specifications of surface roughness measurement system.



Figure 4. MarSurf VD 280 surface roughness measurement system

Table 4. MarSurf VD 280 specifications

S. no.	Specification	MarSurf VD 280
1	Manufacturer	Mahr GmbH, Germany
2	Measurement type	Surface roughness and contour measurement
3	Measurement principle	Tactile, skidless probe system
4	Traversing length	0.1–280 mm
5	Roughness measuring range	Up to ±250 µm with 45-mm probe arm
6	Maximum measuring range	Up to ±750 µm with 135-mm probe arm
7	Resolution	Up to 0.2 nm, depending on measuring range
8	Roughness measuring force	0.75 mN
9	Measurement speed	0.02–10 mm/s
10	*X*-axis positioning speed	0.02–200 mm/s
11	*Z*-axis positioning speed	0.02–50 mm/s
12	Surface parameters considered in present study	Ra and Rz
13	Measurement directions in present study	Two mutually perpendicular directions
14	Evaluation software	MarWin

The experimental evaluation of surface roughness revealed significant variations in the roughness characteristics across the different process parameter combinations, as shown in Table 5. The arithmetical mean height of the roughness profile (Ra) and the maximum height of the roughness profile (Rz) were selected as the surface texture parameters for evaluating the surface quality of the FFF-printed specimens. The definition and determination of Ra as a profile-based surface texture parameter are in accordance with ISO 21920-2:2021 [34]. For reference, the conventional N1–N12 surface-roughness

grade designations correspond to nominal Ra values ranging from 0.025 to 50 μm and are associated with the surface-texture indication framework [35].

Table 5. Experimental values of surface roughness at different regions

Trial no.	A	B (mm)	C (%)	D (°)	E	Ra (μm)	Rz (μm)
1	1	1	1	1	1	6.72	46.87
2	1	1	2	2	2	8.25	51.76
3	1	1	3	3	3	7.76	55.9
4	1	2	1	1	2	5.11	33.27
5	1	2	2	2	3	8.69	56.4
6	1	2	3	3	1	11.97	69.72
7	1	3	1	2	1	9.1	67.65
8	1	3	2	3	2	9.51	62.02
9	1	3	3	1	3	29.72	155.31
10	2	1	1	3	3	12.03	71.77
11	2	1	2	1	1	10.7	68.66
12	2	1	3	2	2	11.55	72.72
13	2	2	1	2	3	23.91	128.1
14	2	2	2	3	1	17.07	93.85
15	2	2	3	1	2	17.23	93.73
16	2	3	1	3	2	20.83	115.63
17	2	3	2	1	3	19.3	105.37
18	2	3	3	2	1	19.43	109.15
		Minimum				5.11	33.27
		Maximum				29.72	155.31
		Average				13.83	80.99

Among the eighteen experimental trials, the lowest values of arithmetical mean height of the roughness profile (Ra) and maximum height of the roughness profile (Rz), measuring 5.11 μm and 33.27 μm, respectively, were obtained for the parameter combination A1B2C1D1E2, corresponding to flat build orientation, 0.17 mm layer thickness, 50% infill density, 0° raster angle, and Triangle infill pattern. In contrast, the highest roughness values of 29.72 μm (Ra) and 155.31 μm (Rz) were observed for the parameter combination A1B3C3D1E3, comprising flat build orientation, 0.24 mm layer thickness, 100% infill density, 0° raster angle, and grid infill pattern.

The relatively poor surface quality observed in certain specimens can primarily be attributed to the staircase effect, which is an inherent limitation of the FFF process. This phenomenon becomes more pronounced with increasing layer thickness, resulting in greater surface irregularities. Furthermore, components fabricated with higher infill densities tend to exhibit inferior top-surface finish due to increased material deposition. Since FFF involves repeated heating and cooling cycles during layer-by-layer fabrication, thicker deposited layers require longer solidification times. The deposition of subsequent layers before complete solidification of the previous layer can lead to uneven material accumulation and increased surface roughness.

Figures 5 and 6 illustrate the surface roughness profiles of specimens fabricated under experimental conditions 4 and 9, respectively, representing the best and worst surface quality outcomes observed in the present study.

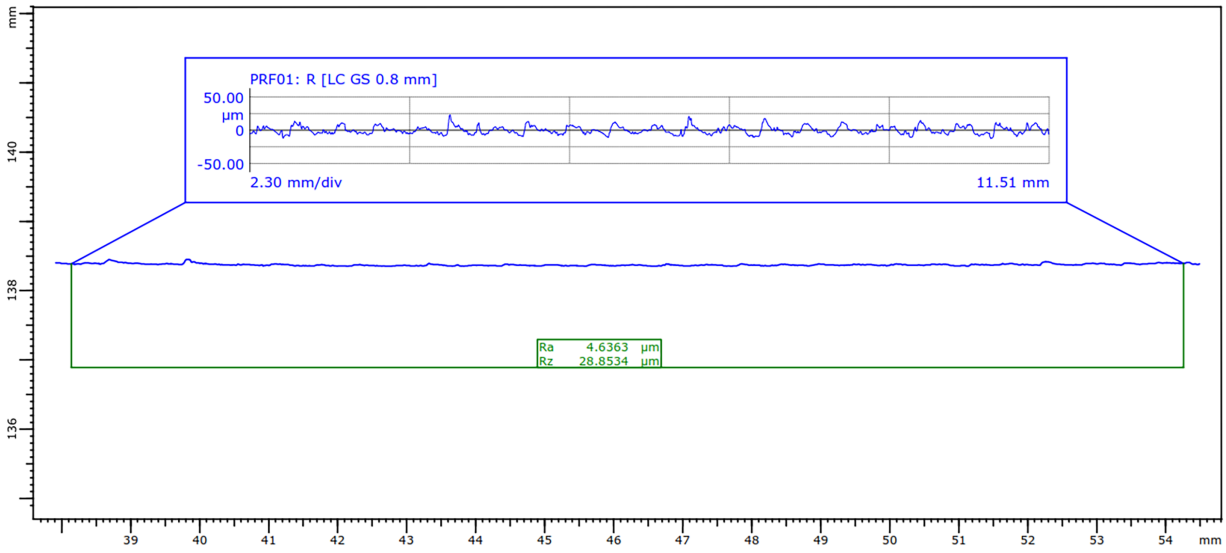


Figure 5. Surface roughness profile of sample 4

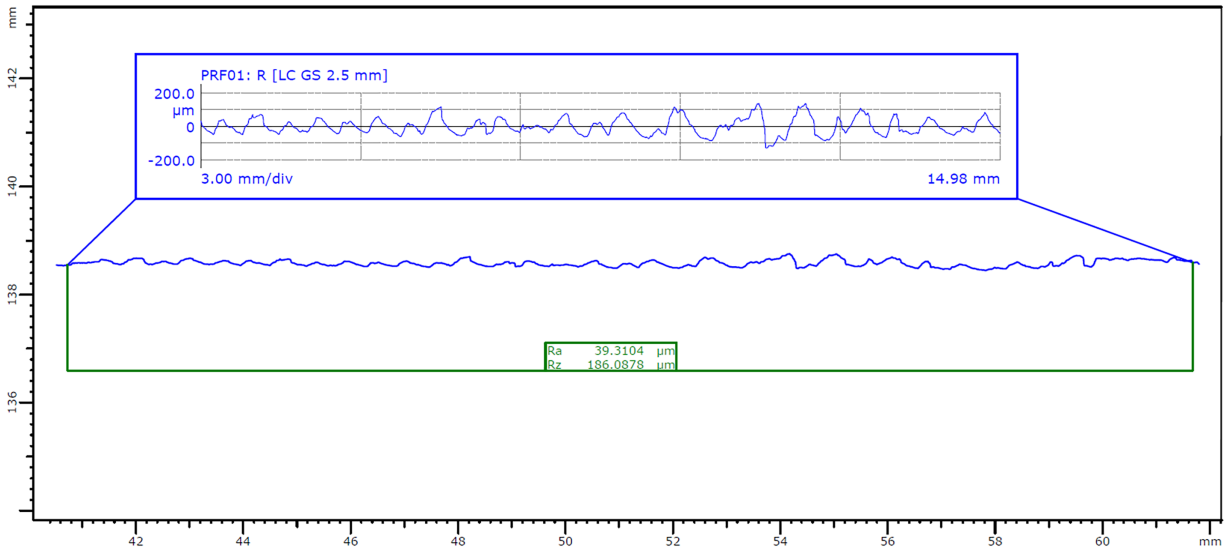


Figure 6. Surface roughness profile of sample 9

4. Results and discussion

Signal-to-noise ratio is a measure of robustness, which can be used to identify the control factor settings that minimize the effect of noise on the response. The present study considers two surface roughness responses, namely the arithmetical mean height of the roughness profile (Ra) and the maximum height of the roughness profile (Rz). Both responses are treated as "smaller-the-better" characteristics, since lower values indicate improved surface quality. Accordingly, the smaller-the-better signal-to-noise (S/N) ratio was calculated separately for Ra and Rz for each experimental trial using Minitab 17.0 software.

$$\text{Signal to Noise Ratio}_{\text{Smaller the Better}} = -10 * \log\left(\sum \frac{Y^2}{n}\right) \quad (1)$$

The main effect plot generated for arithmetical mean height of the roughness profile (Ra) by utilizing signal to noise ratio smaller the better have shown the main effect plot for reducing the same. The

combination A1B1C1D2E2 (Flat orientation, 0.10 mm layer thickness, 50% infill density, 45° Raster angle and Triangle infill pattern) has been recommended for reducing the arithmetical mean height of the roughness profile of the material. The proposed combination of input factor setting is not available with the current experimental trail and from response table ranking's, layer thickness ranks top, and followed by part orientation, infill pattern, infill density and raster angle. Figure 7 shows the main effect plot for reducing arithmetical mean height of the roughness profile (Ra). Table 6 represents the response table rankings for arithmetical mean height of the roughness profile (Ra).

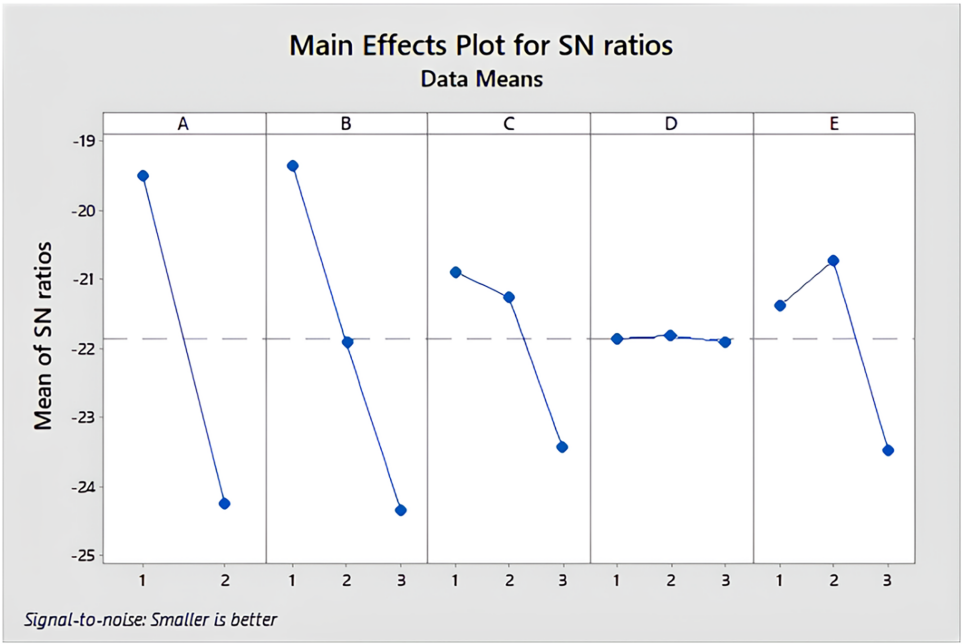


Figure 7. Main effect plot for reducing roughness average

Table 6. Response table ranking's for arithmetical mean height of the roughness profile (Ra)

Level	A	B (mm)	C (%)	D (°)	E
1	−19.49	−19.35	−20.91	−21.87	−21.38
2	−24.25	−21.91	−21.27	−21.81	−20.74
3	–	−24.34	−23.43	−21.92	−23.49
Delta	4.76	4.99	2.52	0.11	2.75
Rank	2	1	4	5	3

On the contrary for reducing maximum height of the roughness profile (Rz), the input factor combination A1B1C1D1E2 (Flat orientation, 0.10 mm layer thickness, 50% infill density, 0° Raster angle and Triangle infill pattern). Layer thickness ranks top and subsequently followed by part orientation, infill pattern, infill density and raster angle. Figure 8 shows the main effect plot for reducing maximum height of the roughness profile (Rz). Table 7 represents the response table rankings for maximum height of the roughness profile (Rz).

The combination recommended through main effect plot for both the roughness characteristics are not available with experimental trail and the same need to be validated through confirmation trials. The optimal factor combination arrived for both the response varies from each other and this stimulates the need for multi criteria decision making.

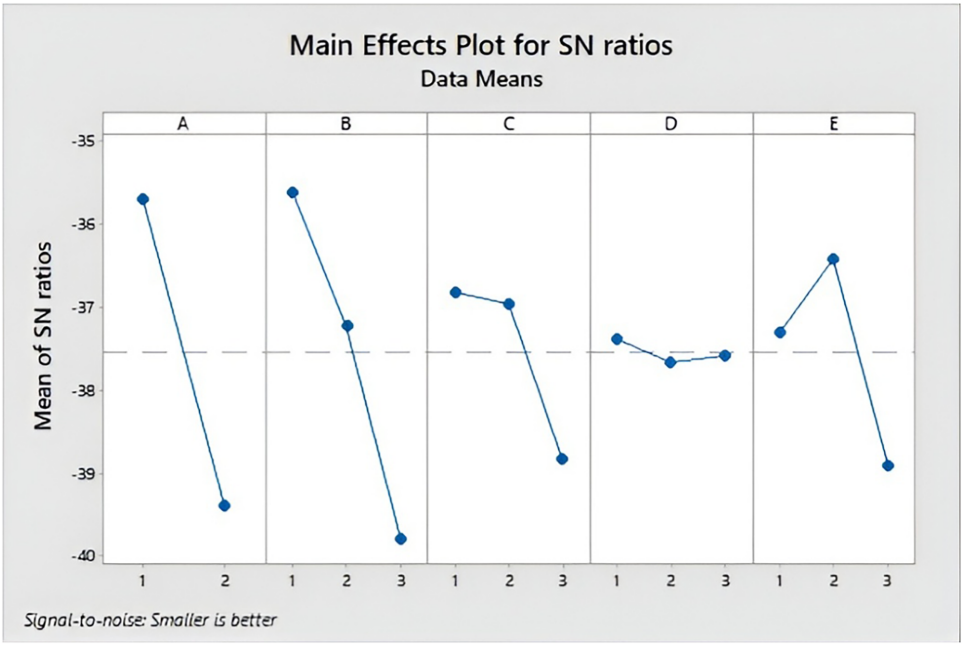


Figure 8. Main effect plot for reducing maximum height of the roughness profile

Table 7. Response table ranking's for maximum height of the roughness profile (Rz)

Level	A	B (mm)	C (%)	D (°)	E
1	−35.7	−35.62	−36.83	−37.38	−37.31
2	−39.4	−37.23	−36.97	−37.68	−36.42
3	–	−39.79	−38.85	−37.58	−38.92
Delta	3.7	4.17	2.01	0.29	2.5
Rank	2	1	4	5	3

The greater influence of layer thickness compared with build orientation can be attributed to both the geometrical characteristics of FFF and the behavior of the carbon-fiber-reinforced nylon employed in this study. Several studies carried out in the past [36–41] has reported a similar influence of layer thickness over surface characteristics and mechanical properties for nylon filaments reinforced with carbon and aramid fibers. The filament consists of a Nylon 6/66 copolymer matrix reinforced with 20% carbon fiber. During extrusion, short carbon fibers may preferentially align along the material deposition direction due to shear-induced orientation within the nozzle. This alignment may improve rigidity and dimensional stability of deposited roads and may reduce surface variations during changes in macroscopic build orientation. Furthermore, carbon-fiber reinforcement may restrict polymer deformation and thermally induced dimensional changes during successive heating and cooling cycles. Therefore, orientation-dependent differences could be less pronounced than those typically encountered in unfilled thermoplastics. The characteristics of the Nylon 6/66 matrix, including melt flow and interlayer bonding, may also contribute to this behavior. In contrast, layer thickness directly governs the geometrical resolution of the deposited layers. Increasing layer thickness enhances the staircase effect and increases peak-to-valley variations, thereby directly influencing both Ra and Rz. Accordingly, layer thickness ranked first for both roughness responses, while build orientation ranked second, confirming that orientation remained influential but was comparatively less dominant.

4.1. Descriptive statistics

The descriptive statistics describe the distribution and variation of the two surface roughness responses, Ra and Rz, of the 18 experimental trials. The Table 8 describes the descriptive statistics of output responses. The mean values were 13.827 μm and 80.993 μm for Ra and Rz, respectively. The median values were 11.760 μm and 70.745 μm, respectively. Trial 9: Higher roughness observations have a moderate effect as indicated by lower median values. Both responses showed considerable variation. The standard deviations were 6.731 μm for Ra and 31.769 μm for Rz. Ra ranged from 5.110 to 29.720 μm and Rz from 33.270 to 155.310 μm. The least values for both responses were observed for Trial 4 (A1B2C1D1E2) which had flat build orientation, layer thickness of 0.17 mm, infill density of 50%, raster angle of 0° and Triangle infill pattern. In contrast, the highest values were obtained for Trial 9 (A1B3C3D1E3) which corresponds to a flat orientation, thickness of the layer equal to 0.24 mm, infill density of 100%, raster angle of 0°, and grid infill pattern. The relative variability was found to be high in both the responses under the investigated process conditions as coefficient of variation was found to be 48.68% for Ra and 39.22% for Rz. The distributions were moderately positively skewed with skewness values of 0.869 for Ra and 0.783 for Rz indicating the presence of some relatively high roughness observations. The interquartile ranges were 9.990 μm for Ra and 44.685 μm for Rz, indicating a relevant dispersion. The descriptive results indicate a considerable variation in surface roughness between experimental conditions and are used as a basis for the following outlier assessment and MANOVA analysis.

Table 8. Descriptive statistics of output responses

Statistical measure	Ra (μm)	Rz (μm)
Number of observations, N	18	18
Mean	13.827	80.993
Standard error of mean	1.586	7.488
Standard deviation	6.731	31.769
Variance	45.303	1009.294
Minimum	5.110	33.270
Maximum	29.720	155.310
Range	24.610	122.040
Median	11.760	70.745
First quartile (Q1)	8.793	57.805
Third quartile (Q3)	18.783	102.490
Interquartile range (IQR)	9.990	44.685
Coefficient of variation (CV)	48.68%	39.22%
Skewness	0.869	0.783
Kurtosis (excess)	0.104	0.185
Sum	248.880	1457.880
95% CI for mean	10.480–17.174	65.195–96.792

4.2. MANOVA

The Multivariate Analysis of Variance (MANOVA) is a statistical method used to evaluate the simultaneous effect of one or more independent factors on multiple dependent responses. Unlike conventional ANOVA, which evaluates the effect of each response separately, MANOVA takes into account the correlation between the dependent variables and evaluates whether the changes in the input factors have a statistically significant combined effect on the responses. In the present study, MANOVA was used to evaluate the simultaneous effects of build orientation, layer thickness, infill

density, raster angle and infill pattern on the surface roughness parameters Ra and Rz. Multivariate significance was assessed using Wilks' Lambda, Pillai's Trace, Lawley–Hotelling Trace, and Roy's Largest Root criteria. A significance level of $p < 0.05$ was adopted to identify statistically significant process parameters. Table 9 represents the outcomes of MANOVA analysis.

Table 9. MANOVA outcomes

Factor	Criterion	Statistic	F	Num DF	Denom DF	*p*-Value	Significance ($p < 0.05$)
A	Wilks'	0.55909	2.76	2	7	0.131	Not significant
A	Lawley-Hotelling	0.78863	2.76	2	7	0.131	Not significant
A	Pillai's	0.44091	2.76	2	7	0.131	Not significant
A	Roy's	0.78863					—
B	Wilks'	0.24526	3.567	4	14	0.033	Significant
B	Lawley-Hotelling	2.18357	3.275	4	12	0.049	Significant
B	Pillai's	0.97394	3.797	4	16	0.023	Significant
B	Roy's	1.63791					—
C	Wilks'	0.74242	0.562	4	14	0.694	Not significant
C	Lawley-Hotelling	0.33906	0.509	4	12	0.731	Not significant
C	Pillai's	0.26343	0.607	4	16	0.664	Not significant
C	Roy's	0.31397					—
D	Wilks'	0.67885	0.748	4	14	0.575	Not significant
D	Lawley-Hotelling	0.46676	0.7	4	12	0.607	Not significant
D	Pillai's	0.32543	0.777	4	16	0.556	Not significant
D	Roy's	0.45282					—
E	Wilks'	0.55471	1.199	4	14	0.354	Not significant
E	Lawley-Hotelling	0.69961	1.049	4	12	0.422	Not significant
E	Pillai's	0.50251	1.342	4	16	0.297	Not significant
E	Roy's	0.48845					—

The multivariate test statistics were interpreted after checking the underlying statistical assumptions to ensure that MANOVA results were valid. The independence of observations was guarantyd by the experimental design, as each experimental trial corresponded to a separately fabricated specimen. Ra and Rz were treated as continuous dependent variables and the studied FFF process parameters as categorical experimental factors. The distributions of the response variables were examined for approximate normality and multivariate outliers were tested for. The relationship between Ra and Rz was studied to determine if there is a problematic multicollinearity. Additionally, the homogeneity of variance-covariance structure was examined between the experimental groups before the interpretation of Wilks' Lambda. The MANOVA results were subsequently interpreted based on the multivariate test statistics and corresponding significance levels.

The MANOVA results were used to test the simultaneous effect of the five FFF process parameters on the two correlated surface roughness responses Ra and Rz as shown in Table 8. Of the factors tested, layer thickness (B) was the only statistically significant parameter at the 95% confidence level. For layer thickness, Wilks' Lambda was 0.2453 with an F-value of 3.567 and $p = 0.033$, which indicates a significant multivariate effect on the combined surface roughness characteristics. This was further confirmed by the Lawley–Hotelling ($p = 0.049$) and Pillai's Trace ($p = 0.023$) tests. The agreement among these multivariate criteria strengthens the evidence that changes in layer thickness significantly alter the overall surface quality.

In contrast, build orientation (A), infill density (C), raster angle (D), and infill pattern (E) produced Wilks' test p-values of 0.131, 0.694, 0.575, and 0.354, respectively, indicating that their combined effects on Ra and Rz were not statistically significant at $p < 0.05$. However, statistical non-significance should not be interpreted as the complete absence of practical influence, particularly considering the relatively small L_{18} experimental design. The dominant influence of layer thickness is physically reasonable because it directly controls the vertical resolution of FFF deposition. The increase in layer thickness leads to an increase in the staircase effect and also increases the magnitude of surface peaks and valleys, thus influencing both Ra and Rz. In general, the MANOVA results statistically corroborate the S/N response analysis, where layer thickness was also the most influential parameter for both roughness characteristics. Hence, the consistency between MANOVA and Taguchi analyses reinforces the conclusion that controlling the layer thickness is particularly important for enhancing the surface quality of the printed carbon-fiber-reinforced nylon components. Table 9 represents the MANOVA results.

5. Multi criteria decision making

The identification of optimal parameter setting that can maximize or decrease an output parameter to a desired value can be processed through multi criteria decision making (MCDM) techniques. Multi-objective optimization combines each individual objective into a combined form. The combined goal ranks the alternatives taken into consideration after taking into account all of the output responses collectively. The weights to be assigned for each unique output response are determined by processing the experimental data, after which multi-objective optimization is used. After the experimental data is processed, the combined objective produces a single value that is known as the multi response performance index. The option ranked top has higher multi-response performance index value.

The current study has considered Shannon's entropy and principal component analysis methods were independently used to determine alternative criteria weight values and TOPSIS has been adopted for ranking the alternatives. The measured outcomes in the current study are arithmetical mean height of the roughness profile (Ra) and maximum height of the roughness profile (Rz) values which fall under the category of minimization for better product quality. The rationale behind considering the comparison of Entropy-TOPSIS and PCA-TOPSIS techniques is due to their strong potential to solve simultaneous optimization problems with a good accuracy. Entropy assigns weights based on information variability, whereas PCA considers correlations among responses through eigenvalue analysis. TOPSIS then ranks the experimental alternatives based on their closeness to the ideal solution. In comparison with techniques such as desirability approach, the comparative MCDM framework requires an additional computational effort which is negligible due to the high degree of correlation in alternative rankings.

5.1. Shannon's entropy method

Entropy method was introduced in the year 1948 by Shannon which normalizes the experimental data through decision matrix and transforms them in to corresponding project outcome [33]. The project outcomes evaluated are utilized for computing the entropy measure and to obtain the objective weights which can provide the weight of output responses. Table 10 shows the normalized values of output responses and its project outcomes.

Table 10. Normalized and project outcome values

Trial no.	A	B (mm)	C (%)	D (°)	E	Normalized		Project outcomes	
						Ra (μm)	Rz (μm)	Ra (μm)	Rz (μm)
1	1	1	1	1	1	0.0270	0.0321	−0.0975	−0.1105
2	1	1	2	2	2	0.0331	0.0355	−0.1129	−0.1185
3	1	1	3	3	3	0.0312	0.0383	−0.1081	−0.1250
4	1	2	1	1	2	0.0205	0.0228	−0.0798	−0.0863
5	1	2	2	2	3	0.0349	0.0387	−0.1171	−0.1258
6	1	2	3	3	1	0.0481	0.0478	−0.1459	−0.1454
7	1	3	1	2	1	0.0366	0.0464	−0.1210	−0.1425
8	1	3	2	3	2	0.0382	0.0425	−0.1247	−0.1343
9	1	3	3	1	3	0.1194	0.1065	−0.2538	−0.2386
10	2	1	1	3	3	0.0483	0.0492	−0.1464	−0.1482
11	2	1	2	1	1	0.0430	0.0471	−0.1353	−0.1439
12	2	1	3	2	2	0.0464	0.0499	−0.1425	−0.1495
13	2	2	1	2	3	0.0961	0.0879	−0.2251	−0.2137
14	2	2	2	3	1	0.0686	0.0644	−0.1838	−0.1766
15	2	2	3	1	2	0.0692	0.0643	−0.1849	−0.1764
16	2	3	1	3	2	0.0837	0.0793	−0.2076	−0.2010
17	2	3	2	1	3	0.0775	0.0723	−0.1983	−0.1899
18	2	3	3	2	1	0.0781	0.0749	−0.1991	−0.1941

Step 1: Normalization of the arrays of decision matrix to obtain normalized values P_{ij}

$$P_{ij} = \frac{X_{ij}}{\sum_{i=1}^{m} X_{ij}} \tag{2}$$

Step 2: Transformation of normalized values to project outcomes
Step 3: Computation of the entropy measure of project outcomes using the following equation

$$E_j = -k \sum_{i=1}^{m} P_{ij} \ln P_{ij} \tag{3}$$

$k = 1/\ln(m)$, m—No of Experimental Trials, $m = 18$ $k = 0.3460$.

Step 4: Defining the objective weight based on the entropy concept

$$W_{ij} = \frac{1 - E_j}{\sum_{j=1}^{n}(1 - E_j)} \tag{4}$$

Tables 11 and 12 show the values of summarized project outcomes and value of $\mathbf{1} - \boldsymbol{E_j}$.

Table 11. Summarized value of project outcomes

Ra (μm)	Rz (μm)
−2.78386	−2.82025

Table 12. Value of $1 - E_j$

Ra (μm)	Rz (μm)
0.036851	0.02426

Note: The sum of $1 - E_j$ is 0.06111.

Tables 11–13 show the summarized values of project outcomes, value of $1 - E_j$ and finally the weight values obtained for surface roughness characteristics. The maximum weightage of 60% (0.60) has been assigned for arithmetical mean height of the roughness profile (Ra) and 40% (0.40) weightage is assigned for maximum height of the roughness profile (Rz). Table 13 shows the weight value of output responses.

Table 13. Weight values of output responses

Ra (μm)	Rz (μm)
0.60	0.40

5.2. Principal component analysis

In the present study, Principal component analysis (PCA) was mainly used to analyze the correlation structure of the two surface-roughness responses, arithmetical mean height of the roughness profile (Ra) and maximum height of the roughness profile (Rz), and to assign the objective weights to each of them. Since only two response variables are considered, PCA does not provide much reduction of the dimensions of the responses but rather transforms the correlated responses into orthogonal principal components and determines the one that explains the maximum proportion of the total variance. In the present analysis, the first principal component (PC1) accounts for 99.7% of the total variance, indicating that the two roughness responses contain a highly similar information structure. The eigenvectors associated with PC1 were therefore used to determine the relative contribution of Ra and Rz for weighting purposes. Based on the squared eigenvector coefficients of PC1, both Ra and Rz obtained an equal weight of 0.50. Thus, PCA is used here primarily as an objective weighting approach based on the variance–correlation structure of the two responses rather than as a dimensionality-reduction technique. Table 14 displays the contributions of the other principal components.

Table 14. Eigen values and proportions for principal components

Principal component	Eigen value	Proportion
First	1.9944	0.997
Second	0.0056	0.003

Table 14 shows the Eigen values and proportions for Principal Components. Table 15 highlights the Eigen vectors and finally the weight values of output responses.

Table 15. Eigen vectors for principal components and contributions

Output parameter	PC1	PC2	Weightage
Ra	0.707	−0.707	0.50
Rz	0.707	0.707	0.50

CC BY

5.3. TOPSIS

Technique for Order Preference by Similarity to Ideal Solution (TOPSIS) is a multi-objective optimization tool which finds the best alternative having shorter distance from positive ideal solution and farther distance from negative ideal solution. Alternatives are ranked by using an overall index calculated based upon the distances from ideal solutions. The current step involves ranking of alternatives through TOPSIS methodology by employing the Entropy-derived and PCA-derived weights independently value of closeness coefficient serves as overall or multi response performance index. Table 16 shows normalized output responses and weighted normalized values as per method, calculated closeness coefficient values and alternative rankings.

Table 16. Normalized and weighted normalized output responses

Trial no.	A	B (mm)	C (%)	D (°)	E	Normalized		Weighted normalized	
						Ra (μm)	Rz (μm)	Ra (μm)	Rz (μm)
1	1	1	1	1	1	0.1036	0.1275	0.0621	0.0510
2	1	1	2	2	2	0.1271	0.1407	0.0763	0.0563
3	1	1	3	3	3	0.1196	0.1520	0.0717	0.0608
4	1	2	1	1	2	0.0787	0.0905	0.0472	0.0362
5	1	2	2	2	3	0.1339	0.1534	0.0803	0.0613
6	1	2	3	3	1	0.1845	0.1896	0.1107	0.0758
7	1	3	1	2	1	0.1402	0.1840	0.0841	0.0736
8	1	3	2	3	2	0.1465	0.1686	0.0879	0.0675
9	1	3	3	1	3	0.4580	0.4223	0.2748	0.1689
10	2	1	1	3	3	0.1854	0.1952	0.1112	0.0781
11	2	1	2	1	1	0.1649	0.1867	0.0989	0.0747
12	2	1	3	2	2	0.1780	0.1977	0.1068	0.0791
13	2	2	1	2	3	0.3684	0.3483	0.2211	0.1393
14	2	2	2	3	1	0.2630	0.2552	0.1578	0.1021
15	2	2	3	1	2	0.2655	0.2549	0.1593	0.1020
16	2	3	1	3	2	0.3210	0.3144	0.1926	0.1258
17	2	3	2	1	3	0.2974	0.2865	0.1784	0.1146
18	2	3	3	2	1	0.2994	0.2968	0.1796	0.1187

STEP 1: Normalization of the decision-matrix.

The normalization formula is given by

$$r_{ij}(\mathrm{x}) = \frac{x_{ij}}{\sqrt{\sum_{i=1}^{m} x_{ij}^2}} i = 1, \ldots, m; j = 1, \ldots, n \tag{5}$$

STEP 2: Calculate the weighted normalized decision matrix.

According to the following formula, the normalized matrix is multiplied by the weight of the criteria.

$$v_{ij}(\mathrm{x}) = w_j r_{ij}(x) i = 1, \ldots, m; j = 1, \ldots, n \tag{6}$$

STEP 3: Determine the positive ideal and negative ideal solutions.

The aim of the TOPSIS method is to calculate the degree of distance of each alternative from positive and negative ideals. Therefore, in this step, the positive and negative ideal solutions are determined according to the following formulas.

So that

$$v_j^+ = \left\{\left(min\ v_{ij}(x)\middle|\, j\ \epsilon\ j_1\right), \left(max\ v_{ij}(x)\middle|\, j\ \epsilon\ j_2\right)\right\}\ i = 1, \ldots, m \tag{7}$$

$$v_j^- = \left\{\left(max\ v_{ij}(x)\middle|\, j\ \epsilon\ j_1\right), \left(min\ v_{ij}(x)\middle|\, j\ \epsilon\ j_2\right)\right\}\ i = 1, \ldots, m \tag{8}$$

where j_1 and j_2 denote the negative and positive criteria, respectively.

STEP4: Euclidean distance from the positive and negative ideal solutions

TOPSIS method ranks each alternative based on the relative closeness degree to the positive ideal and distance from the negative ideal. Therefore, in this step, the calculation of the distances between each alternative and the positive and negative ideal solutions is obtained by using the following formulas.

$$d_i^+ = \sqrt{\sum_{j=1}^{n}[v_{ij}(x) - v_j^+(x)]^2}, i = 1, \ldots, m \tag{9}$$

$$d_i^- = \sqrt{\sum_{j=1}^{n}[v_{ij}(x) - v_j^-(x)]^2}, i = 1, \ldots, m \tag{10}$$

STEP 5: Calculate the relative closeness degree of alternatives to the ideal solution

In this step, the relative closeness degree of each alternative to the ideal solution is obtained by the following formula. If the relative closeness degree has value near to 1, it means that the alternative has shorter distance from the positive ideal solution and longer distance from the negative ideal solution.

$$\mathrm{C}_i = \frac{d_i^-}{(d_i^+ + d_i^-)}, i = 1, \ldots, m \tag{11}$$

The following Table 16 shows the normalized and weighted normalized output responses
Table 17 shows the positive and negative ideal values for the roughness characteristics

Table 17. Positive and negative Ideal values

S. no.	Output response	Positive ideal (v_j^+)	Negative ideal (v_j^-)
1	Ra (μm)	0.0472	0.2748
2	Rz (μm)	0.0362	0.1689

Table 18 represents the relative closeness degree of each alternative to the ideal solution and its ranking.

In the TOPSIS method, the alternative with the highest closeness coefficient (C_i) is considered the most desirable solution, as it is closest to the positive ideal solution and farthest from the negative ideal solution. Conversely, the alternative with the lowest closeness coefficient represents the least favorable combination of process parameters with respect to the combined objectives. Based on the criteria weights obtained through the Entropy method, the ranking order of the experimental alternatives was determined as: 4 > 1 > 3 > 2 > 5 > 8 > 7 > 11 > 12 > 6 > 10 > 14 > 15 > 17 > 18 > 16 > 13 > 9. Similarly, the rankings generated using the weight values derived from Principal Component Analysis (PCA) were found to be: 4 > 1 > 2 > 3 > 5 > 8 > 7 > 11 > 6 > 12 > 10 > 14 > 15 > 17 > 18 > 16 > 13 > 9.

Table 18. Ranking of alternatives through entropy weighted values

Trial no.	d_i^+	d_i^-	C_i	Rank
1	0.0210	0.2432	0.9206	2
2	0.0353	0.2282	0.8660	4
3	0.0347	0.2300	0.8688	3
4	0.0000	0.2634	1.0000	1
5	0.0416	0.2222	0.8424	5
6	0.0748	0.1887	0.7161	10
7	0.0525	0.2132	0.8023	7
8	0.0513	0.2126	0.8056	6
9	0.2634	0.0000	0.0000	18
10	0.0765	0.1871	0.7099	11
11	0.0644	0.1995	0.7559	8
12	0.0734	0.1905	0.7219	9
13	0.2021	0.0613	0.2328	17
14	0.1287	0.1347	0.5114	12
15	0.1299	0.1335	0.5068	13
16	0.1707	0.0928	0.3522	16
17	0.1528	0.1106	0.4198	14
18	0.1560	0.1076	0.4081	15

A comparison of the ranking results obtained from Entropy-TOPSIS and PCA-TOPSIS revealed a strong agreement, with a Pearson correlation coefficient of 99.58%. The minor differences observed in the rankings can be attributed to the slight variation in criteria weights assigned by the two weighting techniques. Figure 9 presents a comparative analysis of the rankings obtained through Entropy-TOPSIS and PCA-TOPSIS approaches.

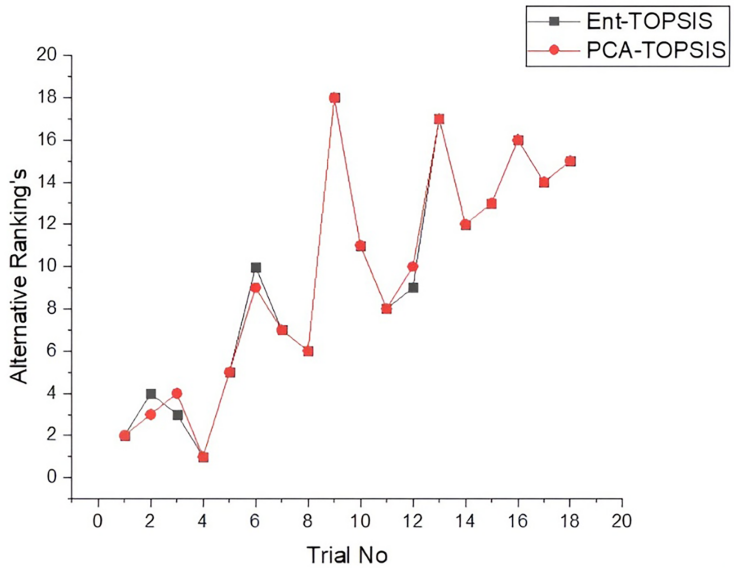


Figure 9. Comparison of alternative ranking from different criteria weight assessment methods

Both methods identified the parameter combination A1B2C1D1E2 (flat build orientation, 0.17 mm layer thickness, 50% infill density, 0° raster angle, and Triangle infill pattern) as the best-performing

alternative for minimizing both arithmetical mean height of the roughness profile (Ra) and maximum height of the roughness profile (Rz). In contrast, the parameter combination A1B3C3D1E3 (flat build orientation, 0.24 mm layer thickness, 100% infill density, 0° raster angle, and grid infill pattern) was ranked as the least favorable alternative, resulting in the highest surface roughness values and consequently deteriorating the overall surface quality of the printed parts. Table 19 presents the alternative rankings obtained through TOPSIS using PCA-derived criteria weights.

Table 19. Ranking of alternatives through PCA weighted values

Trial no.	A	B (mm)	C (%)	D (°)	E	C_i	Rank
1	1	1	1	1	1	0.9119	2
2	1	1	2	2	2	0.8616	3
3	1	1	3	3	3	0.8543	4
4	1	2	1	1	2	1.0000	1
5	1	2	2	2	3	0.8343	5
6	1	2	3	3	1	0.7125	9
7	1	3	1	2	1	0.7802	7
8	1	3	2	3	2	0.7951	6
9	1	3	3	1	3	0.0000	18
10	2	1	1	3	3	0.7037	11
11	2	1	2	1	1	0.7444	8
12	2	1	3	2	2	0.7107	10
13	2	2	1	2	3	0.2305	17
14	2	2	2	3	1	0.5095	12
15	2	2	3	1	2	0.5062	13
16	2	3	1	3	2	0.3458	16
17	2	3	2	1	3	0.4173	14
18	2	3	3	2	1	0.4010	15

To further analyze the multi-response optimization results, the closeness coefficient values obtained from both Entropy-TOPSIS and PCA-TOPSIS methods were subjected to Signal-to-Noise (S/N) ratio analysis using the “higher-the-better” criterion. This approach was adopted to identify the process parameter combination that maximizes the closeness coefficient value and thereby provides the best overall performance with respect to the combined surface roughness objectives.

The main effects plot generated from the S/N ratio analysis indicated that the optimal parameter combination corresponds to A2B1C2D3E2, representing on-edge build orientation, 0.10 mm layer thickness, 75% infill density, 90° raster angle, and a Triangle infill pattern. Among the investigated process parameters, layer thickness emerged as the most influential factor affecting the closeness coefficient value. It was followed in order of significance by infill pattern, infill density, raster angle, and build orientation. Figure 10 illustrates the main effects plot for the closeness coefficient values, while Table 20 presents the response table and the corresponding factor rankings obtained from the S/N ratio analysis.

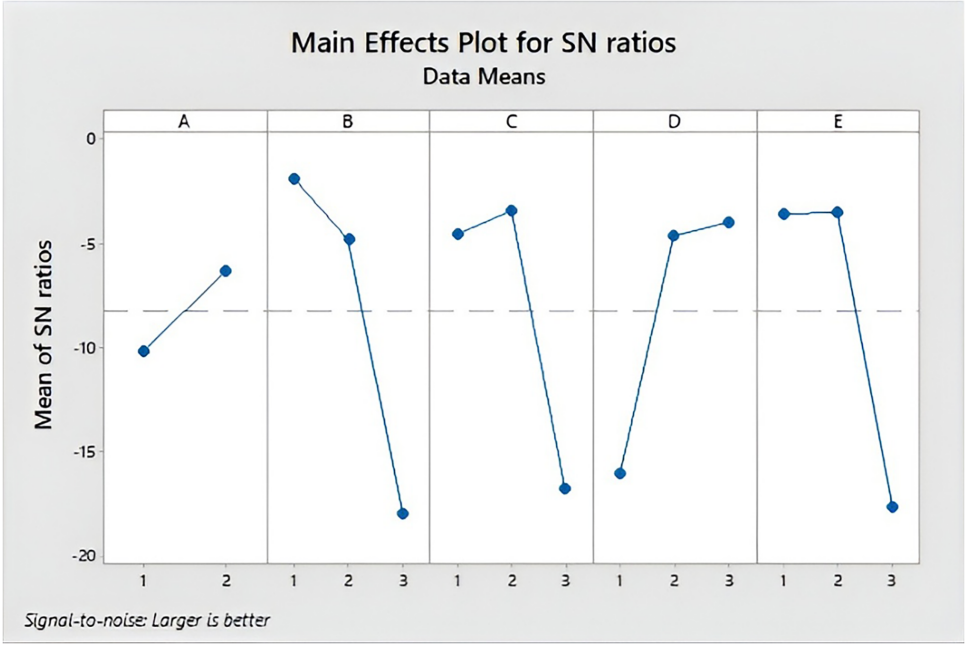


Figure 10. Main effect plot for closeness coefficient values

Table 20. Response table for closeness coefficient value

Level	A	B	C	D	E
1	−10.152	−1.905	−4.555	−16.099	−3.596
2	−6.335	−4.797	−3.402	−4.655	−3.488
3	–	−18.03	−16.773	−3.977	−17.648
Delta	3.817	16.125	13.371	12.121	14.16
Rank	5	1	3	4	2

Figure 11 shows the normal probability plots for closeness coefficient and its shows the normal distribution of residuals. Figures 12 and 13 imply the surface plot generated for closeness coefficient values.

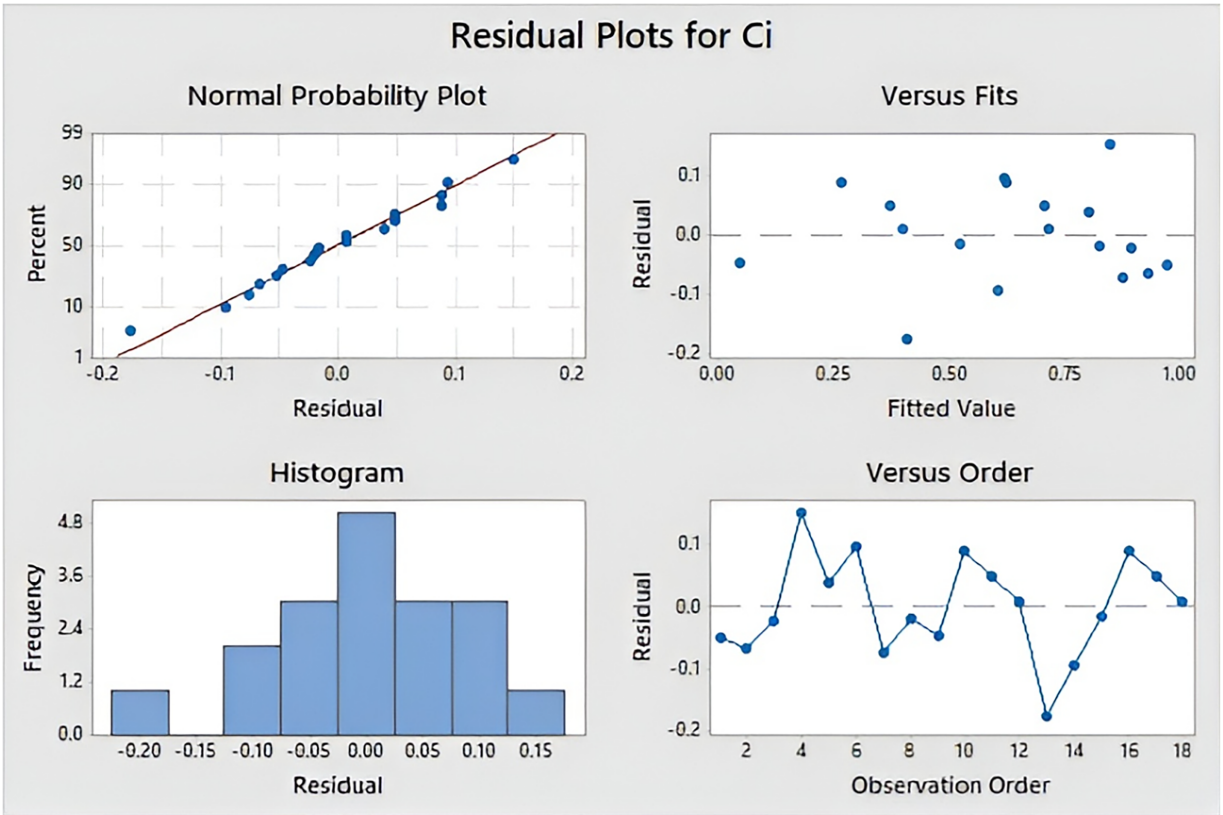


Figure 11. Normal probability plot of residuals

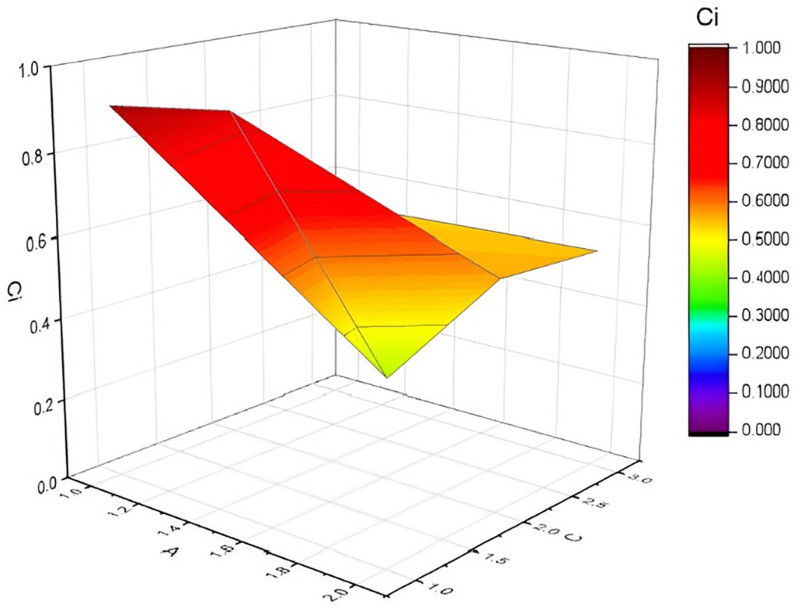


Figure 12. Surface plot between flat orientation and infill density for closeness coefficient values

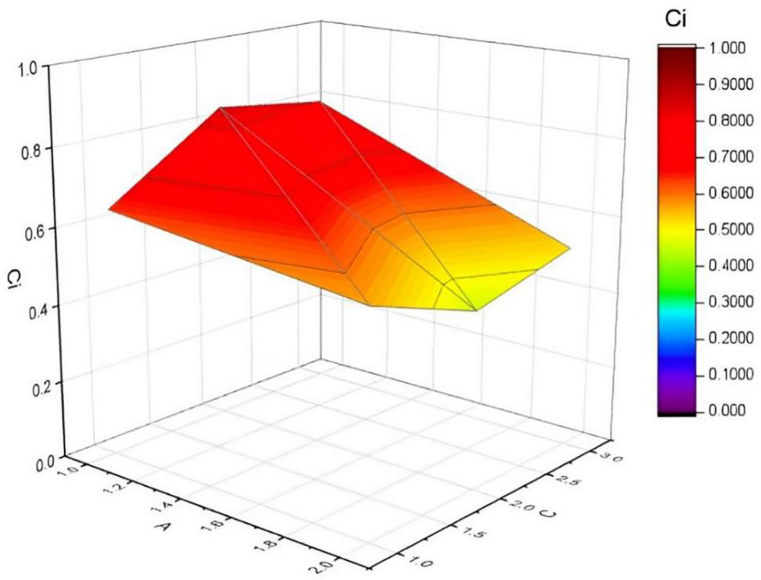


Figure 13. Surface plot between flat orientation and raster angle for closeness coefficient values

Previous research has shown that the surface roughness of FFF is highly influenced by the process parameters, but the significance of each parameter varies depending on the material, the location of the surface, the printing conditions, and the optimization approach. The layer thickness is often known as the dominant factor as the increasing of the layer thickness increases the staircase effect and the height variation between the successive deposited layers. This trend is most prominent for carbon-fiber reinforced nylon. Abas et al. [37] reported that layer height was the most influential parameter on Ra, Rz and Rq for nylon–carbon-fiber components. Part orientation was also found to have a significant effect on surface roughness. The optimum level was found to be 0.10 mm layer height by multi-response optimization. The present study confirms this finding, where the layer thickness was rated as the most significant factor for both Ra and Rz. Differences, however, are present as the present investigation considers build orientation, layer thickness, infill density, raster angle and infill pattern, while Almuflih et al. [40] additionally investigated parameters such as printing speed, extrusion temperature, bed temperature, number of shells and fill angle, evaluating different component surfaces. Hence we expect some variation in the rankings of the factors. The findings of the present study show that build orientation is less important than layer thickness, indicating it has a significant but relatively lower impact. Similar material-specific effect was reported by León-Becerra et al. [42] who studied short carbon-fiber nylon using different build orientations and found a significant effect of orientation on surface roughness with a flat orientation providing favorable surface characteristics. Again, the current study found flat orientation to be advantageous for individual roughness minimization, especially for Trial 4. This agreement demonstrates that the build orientation effect is also valid for carbon-fiber reinforced nylon. Differences are also observed when compared to nylon–aramid composites. Nagendra et al. [39] showed an optimum combination of layer thickness of 0.20 mm, printing temperature of 280°C, raster angle of 90°, tetrahedral infill and infill density of 90%. In contrast, the present study obtained 0.10 mm layer thickness and Triangle infill as favorable conditions. The variations show that the optimum FFF parameters cannot be directly applied to different fiber-reinforced polymer systems. FFF optimization using Taguchi, response surface methodology, evolutionary algorithms and MCDM techniques has also been used by previous researchers. Saad et al. [24] used RSM with PSO and symbiotic organism search for optimization of surface-roughness and other studies have used hybrid MCDM approaches and evolutionary approaches. Chinchanikar et al. [28] showed the applicability of hybrid MCDM technique for multi-objective FFF optimization. The present study builds

on these approaches by combining Taguchi analysis, Entropy and PCA weighting, TOPSIS ranking and regression-based machine learning. The individual-response analysis showed that low layer thickness, flat orientation and Triangle infill were favorable conditions while the multi-response Entropy-TOPSIS and PCA-TOPSIS analyzes showed that A2B1C2D3E2-on-edge orientation, 0.10 mm layer thickness, 75% infill density, 90° raster angle and Triangle infill were the preferred overall combination. Thus, the present results are in good general agreement with previous research in terms of the dominant influence of layer thickness. Differences in optimum orientation, infill density, raster angle and infill pattern show that optimum conditions are material-, surface- and methodology-dependent. This specifies the particular contribution of the present work for 20% carbon fiber reinforced Nylon 6/66.

5.4. Confirmation trials

Validation experiments were designed to validate the optimal process parameter combinations obtained from the individual-response and the multi-response optimization approaches. For minimization of Ra, the Taguchi main-effect analysis suggested A1B1C1D2E2, corresponding to flat build orientation, 0.10 mm layer thickness, 50% infill density, 45° raster angle, and Triangle infill pattern. The estimated Ra for this combination was approximately 3.47 μm. Similarly, the optimum combination for Rz was A1B1C1D1E2, corresponding to flat orientation, 0.10 mm layer thickness, 50% infill density, 0° raster angle, and Triangle infill pattern, for which the estimated Rz was approximately 36.46 μm. These combinations were not included directly among the original L_{18} experimental trials and therefore require independent confirmation experiments. Table 21 shows the outcome of confirmation trials.

Table 21. Confirmation trials

Confirmation trial	Optimization basis	Optimal setting	Predicted value	Experimental value	Error (%)
CT1	Main-effect plot—Ra	A1B1C1D2E2	Ra = 3.47 μm	Ra = 3.54 μm	1.98%
CT2	Main-effect plot—Rz	A1B1C1D1E2	Rz = 36.46 μm	Rz = 37.20 μm	1.99%
CT3	MCDM/TOPSIS + S/N	A2B1C2D3E2	Ra = 8.62 μm/ Rz = 55.43 μm	Ra = 8.80 μm/ Rz = 56.70 μm	2.05%/2.24%

For simultaneous optimization, the S/N analysis of the TOPSIS closeness coefficient identified A2B1C2D3E2 as the preferred combination, corresponding to on-edge build orientation, 0.10 mm layer thickness, 75% infill density, 90° raster angle, and Triangle infill pattern. The estimated Ra and Rz at this condition are approximately 8.62 μm and 55.43 μm, respectively. A confirmation error within 1–3% would indicate close agreement between predicted and measured performance.

Confirmation experiments provided close agreement between the predicted and experimentally measured responses for the selected parameter combinations, with errors ranging from approximately 1.98% to 2.24%. These confirmation results provide preliminary support for the identified parameter settings; however, further replicated experiments are required to establish the robustness and repeatability of the predicted optimum.

5.5. Regression machine learning techniques

Regression algorithms are a class of machine learning techniques that establish a mathematical relationship between input variables and a continuous output variable. The primary objective of regression modeling is to learn patterns from existing data and utilize the developed model to predict outcomes for previously unseen data. In the present study, the closeness coefficient values obtained from the multi-response optimization process were further analyzed using regression-based machine learning algorithms to evaluate their predictive capability and suitability for the available dataset.

Four regression algorithms, namely Decision Tree, Random Forest, Linear Regression, and AdaBoost, were employed to model the closeness coefficient values derived from the Entropy-TOPSIS

method. The Entropy-TOPSIS results were selected for machine learning analysis because the Entropy weighting approach assigned different importance values to the output responses, whereas the PCA-TOPSIS method allocated equal weights to both responses. The experimental dataset consisted of 18 observations, which were divided into training and testing subsets using four different train-test split ratios: 60:40, 70:30, 80:20, and 90:10. The four train-test split ratios were selected to investigate whether predictive performance remained stable under different amounts of training data A k-fold cross valiation with K = 10 has been considered in the analysis. Tables 22–25 represent the various performance values of various algorithms for different split ratios. This analysis was performed to investigate the influence of dataset partitioning on the predictive performance of the selected machine learning models. Figure 14 illustrates the workflow adopted for regression modeling using Orange Data Mining software. The performance of the developed models was evaluated using four widely accepted statistical metrics: Mean Squared Error (MSE), Root Mean Squared Error (RMSE), Mean Absolute Error (MAE), and the coefficient of determination (R2). These metrics were used to assess the prediction accuracy and generalization capability of the regression algorithms. For evaluating the accuracy of the trained models, suitable hyperparameters have been varied to ensure reliability and it is represented in Table 26.

Table 22. Performance values of ML algorithms for 60:40 split ratio

Model	MSE	RMSE	MAE	R-sq
Tree	0.0252	0.1588	0.0889	0.6317
Random forest	0.0238	0.1544	0.1225	0.6517
Linear regression	0.0253	0.1592	0.1284	0.6296
AdaBoost	0.0002	0.0135	0.0054	0.9973

Table 23. Performance values of ML algorithms for 70:30 split ratio

Model	MSE	RMSE	MAE	R-sq
Tree	0.0252	0.1588	0.0889	0.6317
Random forest	0.0202	0.1422	0.0860	0.7046
Linear regression	0.0253	0.1592	0.1284	0.6296
AdaBoost	0.0002	0.0135	0.0054	0.9973

Table 24. Performance values of ML algorithms for 80:20 split ratio

Model	MSE	RMSE	MAE	R-sq
Tree	0.0252	0.1588	0.0889	0.6317
Random forest	0.0273	0.1652	0.1003	0.6010
Linear regression	0.0253	0.1592	0.1284	0.6296
AdaBoost	0.0002	0.0135	0.0054	0.9973

Table 25. Performance values of ML algorithms for 90:10 split ratio

Model	MSE	RMSE	MAE	R-sq
Tree	0.0252	0.1588	0.0889	0.6317
Random forest	0.0239	0.1545	0.1055	0.6512
Linear regression	0.0253	0.1592	0.1284	0.6296
AdaBoost	0.0002	0.0135	0.0054	0.9973

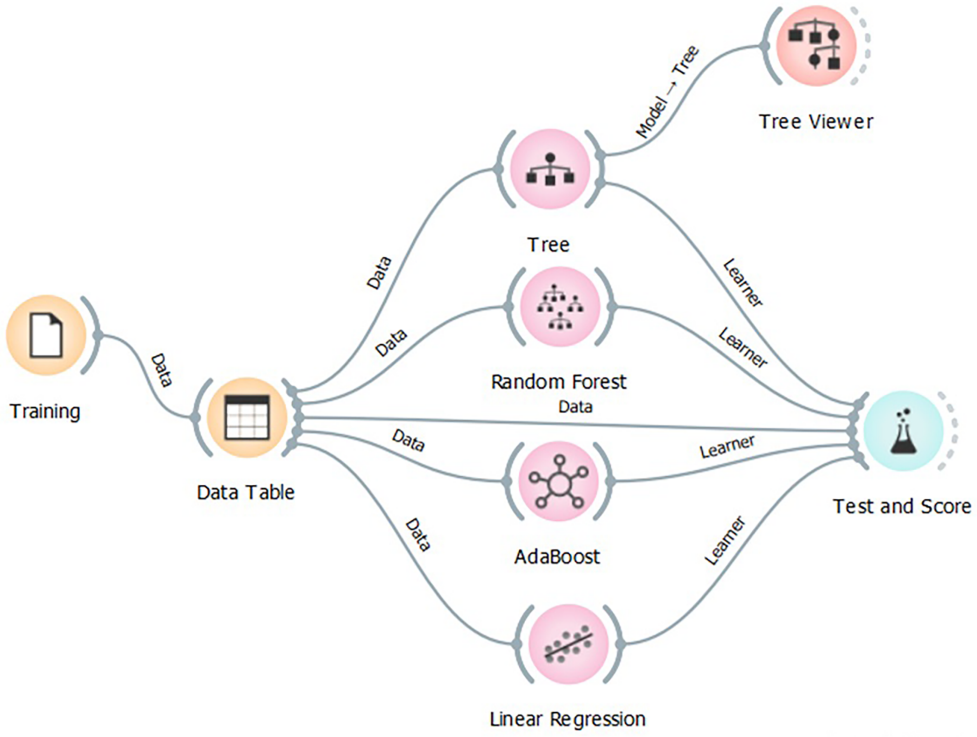


Figure 14. Regression machine learning workflow

Table 26. Hyperparameters tuned for model accuracy improvement

S. no.	ML technique	Hyperparameters
1	Tree	Minimum number of instances in trees = 2 and maximal tree depth = 100
2	Random forest	Number of trees = 20 and limit depth of individual trees = 3
3	Linear regression	Fit intercept = Yes and Regularization = None and Ridge
4	AdaBoost	No. of estimators = 25 and Learning rate = 1.00

The performance evaluation of the selected machine learning algorithms revealed that the AdaBoost regression model consistently outperformed the other algorithms across all train-test split ratios considered in this study. The model achieved superior results for all evaluation metrics, including MSE, RMSE, MAE, and R^2. Furthermore, variations in the train-test split ratio had a negligible effect on its predictive performance. The AdaBoost model attained an R^2 value of approximately 0.99, indicating an excellent fit to the data and a strong capability to accurately predict future outcomes. Additionally, the corresponding MSE, RMSE, and MAE values were considerably lower than those of the other models, further confirming its robustness and prediction accuracy.

In contrast, Linear Regression, Decision Tree, and Random Forest models exhibited comparatively lower predictive performance, with R^2 values consistently below 0.70 across all train-test split ratios. These results suggest that the models were less effective in capturing the underlying relationship between the process parameters and the closeness coefficient values. Moreover, the performance of the Linear Regression and Decision Tree models remained largely unchanged despite increasing the proportion of training data, indicating limited potential for improvement with the current dataset.

The Random Forest model demonstrated a moderate variation in performance with changes in the train-test split ratio. Its predictive accuracy improved when the split ratio was increased from 60:40 to 70:30 but declined slightly at the 80:20 split ratio. A marginal improvement was again observed

when the training dataset was increased to 90% of the total observations. Tables 22–25 summarize the performance metrics of the regression algorithms under different train-test split configurations.

Among the evaluated regression models, AdaBoost exhibited the highest observed predictive performance, reaching an R^2 value of 0.99 under the evaluated data-splitting configuration. Given the small dataset and absence of independent replicated observations, this result should be regarded as an exploratory indication of model performance rather than definitive evidence of generalization capability.

Among the evaluated algorithms, the Decision Tree model offers an additional advantage in terms of interpretability, as it generates a hierarchical tree structure that clearly illustrates the decision-making process required to achieve a specific target outcome. Figure 15 presents the decision tree developed for predicting the closeness coefficient values. The tree consists of 11 nodes and 6 leaf nodes. Build orientation serves as the root node, indicating its role as the primary splitting criterion, followed by layer thickness, infill density, and raster angle as internal decision nodes. The leaf nodes represent the predicted closeness coefficient values corresponding to specific combinations of process parameters, thereby providing a clear understanding of the conditions required to achieve desirable performance levels.

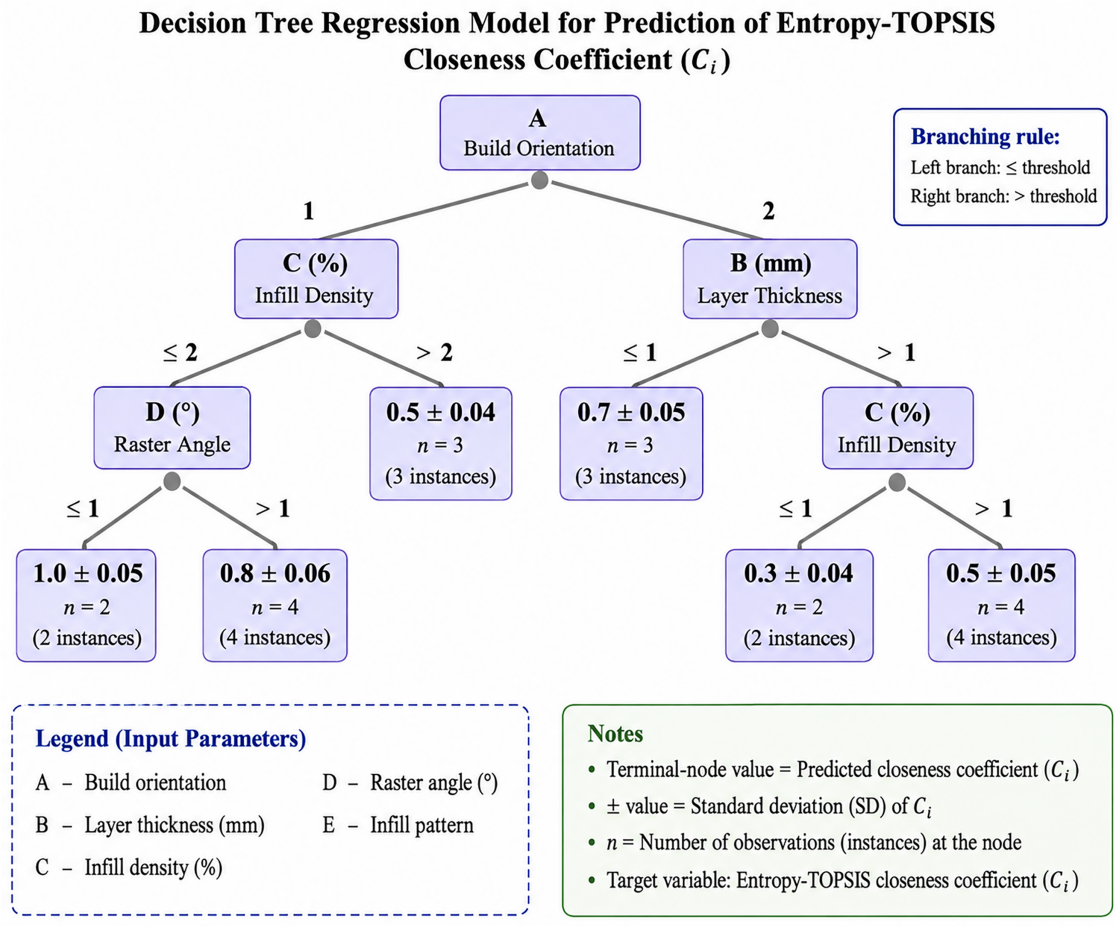


Figure 15. Tree structure for optimal input factor conditions

5.6. Surface characterization

The surface characterization of the printed samples have been performed through Scanning electron Microscope (SEM) technique. The printed samples have been viewed at different magnifications such as 50×, 100×, 250×, 500× and 1000×. Scale factors such as 200 μm, 100 μm, 20 μm and 2 μm

have been fixed to have an in-depth understanding about the surface texture resulted by varying the input factors.

The surface morphology of the printed specimens was examined at different magnifications using SEM analysis to investigate the surface characteristics resulting from the layer-by-layer fabrication process. The micrographs revealed the presence of various surface irregularities inherent to the FFF process. At a magnification of 150×, the deposited layers were clearly distinguishable, and noticeable gaps between adjacent layers could be observed. The layers also exhibited irregular geometrical profiles, indicating non-uniform material deposition during printing.

At a higher magnification of 500×, the surface features became more prominent, revealing material accumulations and protrusions caused by uneven heating and cooling cycles during the printing process. Such irregularities can be attributed to the thermal history of the deposited material, where successive layers are deposited before the complete solidification of the underlying layers. This phenomenon becomes more pronounced at higher layer thicknesses, as thicker layers require longer cooling and solidification times. Consequently, incomplete solidification and subsequent material deposition can lead to surface defects and increased roughness.

Figures 16 and 17 present the SEM micrographs of the printed specimens at different magnifications, highlighting the surface texture and irregularities produced under the selected printing conditions.

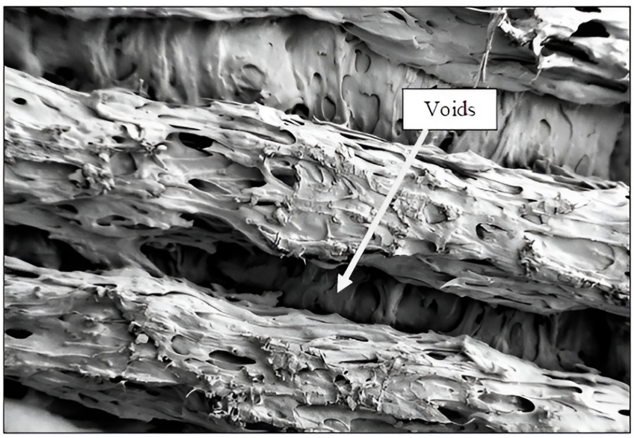


Figure 16. Surface profile of printed samples at 150×

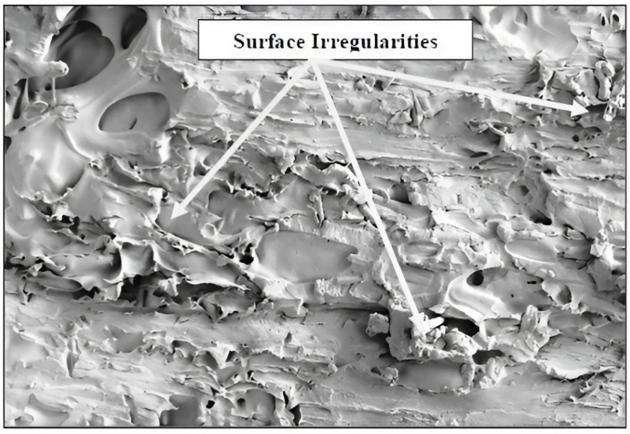


Figure 17. Surface profile of printed samples at 500×

SEM observations provide clear morphological support to the experimentally measured surface roughness of the FFF-printed carbon-fiber-reinforced nylon specimens. The experimental results showed that the Trial 4 with a flat build orientation, 0.17 mm layer thickness, 50% infill density, 0° raster angle, and Triangle infill pattern had the lowest surface roughness with Ra of 5.11 μm and Rz of 33.27 μm. Conversely, the highest Ra and Rz values of 29.72 μm and 155.31 μm, respectively, were obtained for Trial 9, which was printed flat with 0.24 mm layer thickness, 100% infill density, 0° raster angle, and grid infill pattern. The SEM micrographs show typical features of the FFF process such as boundaries of deposited layers, voids between neighboring tracks, irregular geometries, accumulation of material and local protrusions. These morphological features are in good agreement with the observed roughness variations. Trial 4 has relatively low roughness due to controlled deposition of material and reduction in surface height variations. However, the thicker layer thickness of 0.24 mm in Trial 9 worsens the staircase effect and the height difference between the consecutive deposited layers. Also, 100% infill density increases the amount of deposited material, which can cause local material build-up and surface irregularities.

SEM at higher magnification such as 500× shows that the repeated heating and cooling cycles of the FFF process lead to protrusions and unevenly deposited regions. The larger the size of the layer, the longer it takes to cool and solidify. This can cause the next layer to be deposited before the previous layer has fully solidified. This explains the significantly higher Rz of Trial 9, where pronounced peaks and valleys are formed. Therefore, the SEM morphology qualitatively supports the profilometer measurements and confirms the strong influence of printing conditions, particularly layer thickness, on the resulting surface quality.

6. Conclusion

The present study focused on minimizing the surface roughness of FFF-printed nylon composites reinforced with 20% carbon fiber by investigating the influence of build orientation, layer thickness, infill density, raster angle, and infill pattern. Surface roughness measurements were performed using a MarSurf VD 280 system, and the obtained results were analyzed using Signal-to-Noise (S/N) ratio analysis, Multi-Criteria Decision-Making (MCDM) techniques, and machine learning algorithms. The major findings of the study are summarized as follows:

- The measured roughness values were averaged and analyzed using the S/N ratio method with the "smaller-the-better" quality characteristic. The parameter combination A1B1C1D2E2 (flat orientation, 0.10 mm layer thickness, 50% infill density, 45° raster angle, and Triangle infill pattern) was identified as the optimum setting for minimizing Ra, whereas A1B1C1D1E2 (flat orientation, 0.10 mm layer thickness, 50% infill density, 0° raster angle, and Triangle infill pattern) was found to be the optimal combination for minimizing Rz.
- In the explored L18 experimental design space, the response-table analysis showed that the layer thickness is the factor that produced the largest main-effect variation in both Ra and Rz. This was also reflected in the MANOVA results, but since independent replication of specimens was not performed, statistical significance should be interpreted with caution and does not provide a direct estimate of pure experimental error.
- Entropy-based criteria weighting assigned importance values of 60% and 40% to Ra and Rz, respectively. In contrast, Principal Component Analysis (PCA) assigned equal weights of 50% to both responses.
- The alternative rankings obtained through Entropy-TOPSIS and PCA-TOPSIS exhibited strong agreement, with a correlation of 99.58%. Both approaches identified the parameter combination A2B1C2D3E2 (on-edge orientation, 0.10 mm layer thickness, 75% infill density, 90° raster angle, and Triangle infill pattern) as the most suitable setting for maximizing the closeness coefficient value. Layer thickness was again found to be the most significant factor influencing overall performance.

- The application of regression-based machine learning algorithms to predict the closeness coefficient values demonstrated that the AdaBoost algorithm outperformed the other models considered. The model achieved the highest prediction accuracy, with an R^2 value of 0.99 across the different train-test split ratios evaluated.
- SEM-based surface characterization revealed the presence of voids, layer gaps, and other surface irregularities inherent to the layer-by-layer deposition mechanism of the FFF process.
- Confirmation experiments conducted using the optimal parameter combinations obtained from the different optimization techniques validated the effectiveness and reliability of the proposed methodology in identifying suitable process settings for enhanced surface quality.
- The proposed optimization framework offers practical industrial potential for manufacturing lightweight CF-nylon gears, brackets, jigs and fixtures by balancing improved surface quality with reduced material consumption, printing time, post-processing requirements, and overall production cost.
- The future research would consider a comparative study about the effect of fiber content with different fractions ranging from 2% to 20% over mechanical and quality characteristics of the printed samples. Additionally, multiple MCDM techniques for ranking the alternatives will be considered for assessing the robustness of the ranking obtained.

Overall, the integration of Taguchi design, MCDM techniques, and machine learning algorithms proved to be an effective framework for optimizing surface roughness and predicting performance outcomes in FFF-printed carbon fiber reinforced nylon composites.

Acknowledgement: We want to extend our sincere gratitude to everyone who helped with this study endeavor. We would like to thank our friends and colleagues of PSG College of Technology and EASA College of Engineering and Technology for their crucial advice and assistance throughout the research.

Funding Statement: The authors received no specific funding for this study.

Author Contributions: Subhash Selvaraj: conceptualization, methodology, analysis, and investigation. Rajesh P. K.: supervision, project administration, resources, validation. All authors reviewed and approved the final version of the manuscript.

Availability of Data and Materials: The datasets generated and analyzed during the current study are available from the corresponding author.

Ethics Approval: Not applicable.

Conflicts of Interest: The authors declare no conflicts of interest.

References

1. Dey A, Yodo N. A systematic survey of FDM process parameter optimization and their influence on part characteristics. J Manuf Mater Process. 2019;3(3):64. doi:10.3390/jmmp3030064.
2. Penumakala PK, Santo J, Thomas A. A critical review on the fused deposition modeling of thermoplastic polymer composites. Compos Part B Eng. 2020;201(7):108336. doi:10.1016/j.compositesb.2020.108336.
3. Liu Z, Wang Y, Wu B, Cui C, Guo Y, Yan C. A critical review of fused deposition modeling 3D printing technology in manufacturing polylactic acid parts. Int J Adv Manuf Technol. 2019;102(9):2877–89. doi:10.1007/s00170-019-03332-x.
4. Rahim TNAT, Abdullah AM, Md Akil H. Recent developments in fused deposition modeling-based 3D printing of polymers and their composites. Polym Rev. 2019;59(4):589–624. doi:10.1080/15583724.2019.1597883.

5. Gurrala PK, Regalla SP. Multi-objective optimisation of strength and volumetric shrinkage of FDM parts: a multi-objective optimization scheme is used to optimize the strength and volumetric shrinkage of FDM parts considering different process parameters. Virtual Phys Prototyp. 2014;9(2):127–38. doi:10.1080/17452759.2014.898851.
6. Lim GD, Abd Latif MJ, Alkahari MR, Yob MS, Musa M, Abdul Rahman MN, et al. Parameter optimization of fused deposition modeling process for 3D printed prosthetic socket using PCR-TOPSIS method. Int J Nanoelectron Mater. 2022;15:247–58.
7. Saad MS, Mohd Nor A, Zakaria MZ, Baharudin ME, Yusoff WS. Modelling and evolutionary computation optimization on FDM process for flexural strength using integrated approach RSM and PSO. Prog Addit Manuf. 2021;6(1):143–54. doi:10.1007/s40964-020-00157-z.
8. Tura AD, Mamo HB, Gemechu WF. Mathematical modeling and parametric optimization of surface roughness for evaluating the effects of fused deposition modeling process parameters on ABS material. Int J Adv Eng Res Sci. 2021;8(5):49–57. doi:10.22161/ijaers.85.7.
9. Chohan JS, Kumar R, Yadav A, Chauhan P, Singh S, Sharma S, et al. Optimization of FDM printing process parameters on surface finish, thickness, and outer dimension with ABS polymer specimens using taguchi orthogonal array and genetic algorithms. Math Probl Eng. 2022;2022(2):2698845. doi:10.1155/2022/2698845.
10. Chen A, Chen JC. Optimization of surface roughness in additive manufacturing processes via Taguchi methodology. Int J Ind Manuf Eng. 2018;12(4):370–4.
11. Agarwal KM, Shubham P, Bhatia D, Sharma P, Vaid H, Vajpeyi R. Analyzing the impact of print parameters on dimensional variation of ABS specimens printed using fused deposition modelling (FDM). Sens Int. 2022;3(2):100149. doi:10.1016/j.sintl.2021.100149.
12. Park JM, Jeon J, Koak JY, Kim SK, Heo SJ. Dimensional accuracy and surface characteristics of 3D-printed dental casts. J Prosthet Dent. 2021;126(3):427–37. doi:10.1016/j.prosdent.2020.07.008.
13. Noriega A, Blanco D, Alvarez BJ, Garcia A. Dimensional accuracy improvement of FDM square cross-section parts using artificial neural networks and an optimization algorithm. Int J Adv Manuf Technol. 2013;69(9):2301–13. doi:10.1007/s00170-013-5196-2.
14. Chohan JS, Mittal N, Singh R, Singh U, Salgotra R, Kumar R, et al. Predictive modeling of surface and dimensional features of vapour-smoothened FDM parts using self-adaptive cuckoo search algorithm. Prog Addit Manuf. 2022;7(5):1023–36. doi:10.1007/s40964-022-00277-8.
15. Chohan JS, Kumar R, Bhatia Singh THB, Singh S, Sharma S, Singh J, et al. Taguchi S/N and TOPSIS based optimization of fused deposition modelling and vapor finishing process for manufacturing of ABS plastic parts. Materials. 2020;13(22):5176. doi:10.3390/ma13225176.
16. Shah V, Kumar R, Chohan JS. A review on surface enhancement approaches for thermoplastics developed through fused deposition modeling. Eur J Mol Clin Med. 2020;7(7):4485–97.
17. Lukic D, Cep R, Vukman J, Antic A, Djurdjev M, Milosevic M. Multi-criteria selection of the optimal parameters for high-speed machining of aluminum alloy Al7075 thin-walled parts. Metals. 2020;10(12):1570. doi:10.3390/met10121570.
18. Srivastawa A, Maity SR, Pandey KM. Material selection of gear using grey TOPSIS and COPRAS-G method. Int J Biotechnol Biomed Sci. 2017;3(1):34–8.
19. Raigar J, Sharma VS, Srivastava S, Chand R, Singh J. A decision support system for the selection of an additive manufacturing process using a new hybrid MCDM technique. Sādhanā. 2020;45(1):101. doi:10.1007/s12046-020-01338-w.
20. Wang CN, Chung YC, Wibowo FD, Dang TT, Nguyen NAT. Site selection of solar power plants using hybrid MCDM models: a case study in Indonesia. Energies. 2023;16(10):4042. doi:10.3390/en16104042.

21. Marqués AI, García V, Sánchez JS. Ranking-based MCDM models in financial management applications: analysis and emerging challenges. Prog Artif Intell. 2020;9(3):171–93. doi:10.1007/s13748-020-00207-1.
22. Wakchaure KN, Thakur AG, Gadakh V, Kumar A. Multi-objective optimization of friction stir welding of aluminium alloy 6082-T6 using hybrid taguchi-grey relation analysis—ANN method. Mater Today Proc. 2018;5(2):7150–9. doi:10.1016/j.matpr.2017.11.380.
23. Prabhu S, Uma M, Jaishwin J, Nikhil M. Experimental study and predictive modelling of fused deposition modelling (FDM) using TOPSIS and fuzzy logic expert system. Int J Automot Mech Eng. 2023;20(1):10175–91. doi:10.15282/ijame.20.1.2023.03.0788.
24. Saad MS, Nor AM, Baharudin ME, Zakaria MZ, Aiman AF. Optimization of surface roughness in FDM 3D printer using response surface methodology, particle swarm optimization, and symbiotic organism search algorithms. Int J Adv Manuf Technol. 2019;105(12):5121–37. doi:10.1007/s00170-019-04568-3.
25. Mohanty A, Nag KS, Bagal DK, Barua A, Jeet S, Mahapatra SS, et al. Parametric optimization of parameters affecting dimension precision of FDM printed part using hybrid Taguchi-MARCOS-nature inspired heuristic optimization technique. Mater Today Proc. 2022;50(9–12):893–903. doi:10.1016/j.matpr.2021.06.216.
26. Qin Y, Qi Q, Shi P, Scott PJ, Jiang X. Selection of materials in metal additive manufacturing via three-way decision-making. Int J Adv Manuf Technol. 2023;126(3):1293–302. doi:10.1007/s00170-023-10966-5.
27. Vinodh S, Shinde P. Parametric optimization of 3D printing process using MCDM method. In: Precision product-process design and optimization. Singapore: Springer; 2018. p. 141–59. doi:10.1007/978-981-10-8767-7_6.
28. Chinchanikar S, Shinde S, Shaikh A, Gaikwad V, Ambhore NH. Multi-objective optimization of FDM using hybrid genetic algorithm-based multi-criteria decision-making (MCDM) techniques. J Inst Eng Ind Ser D. 2023;105(1):49–63. doi:10.1007/s40033-023-00459-w.
29. Rajamani D, Balasubramanian E, Yang LJ. Enhancing the surface quality of FDM processed flapping wing micro mechanism assembly through RSM–TOPSIS hybrid approach. Processes. 2022;10(11):2457. doi:10.3390/pr10112457.
30. Sakthivel Murugan R, Vinodh S. Parametric optimization of fused deposition modelling process using Grey based Taguchi and TOPSIS methods for an automotive component. Rapid Prototyp J. 2021;27(1):155–75. doi:10.1108/rpj-10-2019-0269.
31. Mohammed Raffic N, Ganesh Babu K, Saminathan R, Hadidi H. Dimensional error minimization through parameter optimization for 3D printed nylon aramid composites using SWARA-CoCoSo and machine learning algorithms. J Mater Eng Perform. 2023;32(24):11326–46. doi:10.1007/s11665-023-08608-8.
32. Selvaraj S, Rajesh PK. Prediction of optimal parameter settings and significant parameter for reduced geometric deviations through multi criteria decision making and machine learning algorithms. Mater Plast. 2024;61(1):43–65. doi:10.37358/mp.24.1.5702.
33. Mohammed Raffic N, Ganesh Babu K, Dharani Kumar S, Parrthipan BK. Surface roughness and printing time minimization in 3D printed aramid fiber reinforced polyamide parts through taguchi-CoCoSo-machine learning techniques. J Mater Eng Perform. 2025;34(11):9654–80. doi:10.1007/s11665-025-11288-1.
34. ISO 21920-2:2021. Geometrical product specifications (GPS)—surface texture: profile—part 2: terms, definitions and surface texture parameters. Geneva, Switzerland: International Organization for Standardization; 2021.

35. ISO 21920-1:2021. Geometrical product specifications (GPS)—surface texture: profile—part 1: indication of surface texture. Geneva, Switzerland: International Organization for Standardization; 2021.
36. Mohammed Raffic N, Ganesh Babu K, Dharani Kumar S, Parrthipan BK. On search of optimal FDM parameter settings for reduced dimensional error using entropy-PCA-TOPSIS and regression machine learning techniques. Proc Inst Mech Eng Part L J Mater Des Appl. 2025;239(3):617–37. doi:10.1177/14644207241312082.
37. Abas M, Awadh MA, Habib T, Noor S. Analyzing surface roughness variations in material extrusion additive manufacturing of nylon carbon fiber composites. Polymers. 2023;15(17):3633. doi:10.3390/polym15173633.
38. Sandeep, Chhabra D, Gupta RK. Optimization of FDM printing parameters for surface quality improvement of carbon based nylon (PA-CF) composite material fabricated parts using evolutionary algorithm. J Nano Electron Phys. 2021;13(2):02004. doi:10.21272/jnep.13(2).02004.
39. Nagendra J, Srinath MK, Sujeeth S, Naresh KS, Ganesha Prasad MS. Optimization of process parameters and evaluation of surface roughness for 3D printed nylon-aramid composite. Mater Today Proc. 2021;44(3):674–82. doi:10.1016/j.matpr.2020.10.609.
40. Almuflih AS, Abas M, Khan I, Noor S. Parametric optimization of FDM process for PA12-CF parts using integrated response surface methodology, grey relational analysis, and grey wolf optimization. Polymers. 2024;16(11):1508. doi:10.3390/polym16111508.
41. Ulkir O, Kuncan F, Alay FD. Experimental study and ANN development for modeling tensile and surface quality of fiber-reinforced nylon composites. Polymers. 2025;17(11):1528. doi:10.3390/polym17111528.
42. León-Becerra J, Hidalgo-Salazar MÁ, Correa-Aguirre JP, González-Estrada OA, Pertuz AD. Additive manufacturing of short carbon filled fiber nylon: effect of build orientation on surface roughness and viscoelastic behavior. Int J Adv Manuf Technol. 2024;130(1):425–35. doi:10.1007/s00170-023-12503-w.

Received: 18 June 2026; Accepted: 02 September 2026; Published: XX XX 2026